

Assessing the C/O Ratio Formation Diagnostic: A Potential Trend with Companion Mass

KIELAN K. W. HOCH,^{1,2} QUINN M. KONOPACKY,¹ CHRISTOPHER A. THEISSEN,^{1,*} JEAN-BAPTISTE RUFFIO,¹
TRAVIS S. BARMAN,³ EMILY L. RICKMAN,⁴ MARSHALL D. PERRIN,² BRUCE MACINTOSH,⁵ AND CHRISTIAN MAROIS⁶

¹*Center for Astrophysics and Space Sciences, University of California, San Diego, La Jolla, CA 92093, USA*

²*Space Telescope Science Institute, 3700 San Martin Dr, Baltimore, MD 21218, USA*

³*Lunar and Planetary Laboratory, University of Arizona, Tucson, AZ 85721, USA*

⁴*European Space Agency (ESA), ESA Office, Space Telescope Science Institute, Baltimore, MD 21218, USA*

⁵*Kavli Institute for Particle Astrophysics and Cosmology, Stanford University, Stanford, CA 94305, USA*

⁶*NRC Herzberg Astronomy and Astrophysics, 5071 West Saanich Rd, Victoria, BC V9E 2E7, Canada*

ABSTRACT

The carbon-to-oxygen (C/O) ratio in an exoplanet atmosphere has been suggested as a potential diagnostic of planet formation. Now that a number of exoplanets have measured C/O ratios, it is possible to examine this diagnostic at a population level. Here, we present an analysis of currently measured C/O ratios of directly imaged and transit/eclipse planets. First, we derive atmospheric parameters for the substellar companion HD 284149 AB b using data taken with the OSIRIS integral field spectrograph at the W.M. Keck Observatory and report two non-detections from our ongoing imaging spectroscopy survey with Keck/OSIRIS. We find an effective temperature of $T_{\text{eff}} = 2502$ K, with a range of 2291–2624 K, $\log g = 4.52$, with a range of 4.38–4.91, and $[M/H] = 0.37$, with a range of 0.10–0.55. We derive a C/O of $0.59^{+0.15}_{-0.30}$ for HD 284149 AB b. We add this measurement to the list of C/O ratios for directly imaged planets and compare them with those from a sample of transit/eclipse planets. We also derive the first dynamical mass estimate for HD 284149 AB b, finding a mass of $\sim 28 M_{\text{Jup}}$. There is a trend in C/O ratio with companion mass (M_{Jup}), with a break seen around $4 M_{\text{Jup}}$. We run a Kolmogorov-Smirnov and an Anderson-Darling test on planets above and below this mass boundary, and find that they are two distinct populations. This could be additional evidence of two distinct populations possibly having two different formation pathways, with companion mass as an indicator of most likely formation scenario.

Keywords: Direct imaging; exoplanet atmospheres; high resolution spectroscopy; exoplanet formation

1. INTRODUCTION

Over 5,000 exoplanets are now known, and only about 80 of these objects have atmospheric data from the Hubble Space Telescope (HST), the Spitzer Space Telescope, and/or various ground-based observatories. There are a few main methods to obtain atmospheric information on these companions, such as direct imaging and the transit or eclipse techniques (Sing et al. 2016; Tsiaras et al. 2018; Pinhas et al. 2019; Mansfield et al. 2021). Direct imaging surveys have revealed a unique population of massive, widely separated exoplanets (Rameau et al. 2013; Biller et al. 2013; Galicher et al. 2016; Nielsen

et al. 2019; Vigan et al. 2021). Revealing these gas giant companions has inspired a number of novel and complex theories to explain their large sizes and separations, such as core/pebble accretion (Johansen & Lambrechts 2017), dynamical scattering (Rasio & Ford 1996; Weidenschilling & Marzari 1996; Chatterjee et al. 2008), disk instability (Kuiper 1951; Cameron 1978), and cloud fragmentation (Toomre 1964). These objects still remain a mystery for many of in situ formation mechanisms.

Most transiting or eclipsing gas giant planets with spectral information are “Hot Jupiters” with temperatures around 1000–2500 K. They orbit close to their host stars (<1 au), and can have a variety of masses spanning from a percent of a Jupiter mass to 30 Jupiter masses. They are thought to form through a three step process starting from core accretion, then runaway gas

Corresponding author: Kielan K. W. Hoch
khoch@stsci.edu

* NASA Sagan Fellow

accretion to form the atmosphere, and finally inward migration to replicate what we see today (Mizuno et al. 1980; Bodenheimer & Pollack 1986; Ikoma et al. 2000). The core accretion step is thought to occur in beyond the ice line of a protoplanetary disk where an abundance of solid material leads to rapid growth of a planetary core before gas dispersal in the disk. With this scenario in mind, the composition of these exoplanets should be sub-stellar in carbon and oxygen because they would be sequestered in the solid core. However, measured bulk metallicities of Jupiter, Saturn, and some exoplanets are shown to be super-stellar, which complicates tracing the formation scenario from composition of the atmospheres (Li et al. 2020; Wong et al. 2004; Visscher & Fegley 2005; Madhusudhan et al. 2011b).

Relative abundance measurements of molecules were first done on transiting Hot Jupiters to characterize their atmospheric temperature and pressure structures (Fortney et al. 2010). In particular, carbon-to-oxygen ratios (C/O) were measured and they differed from their host star significantly, furthering the need for a possible explanation (e.g. WASP-12b, C/O \approx 1; Madhusudhan et al. 2011c). Öberg et al. (2011) engineered a framework to use the C/O ratio to trace how and where the object formed in the protoplanetary disk. In summary, a stellar C/O ratio is expected for companions forming through gravitational instabilities in the disk, where all material is mixed, and for planets forming interior to both the water snow-line and the carbon-grain evaporation line. Superstellar C/O ratios could indicate atmosphere formation from mainly gas accretion outside of the water snowline, possibly via core accretion. Other studies also connected the C/O ratio to formation mechanisms and evolution in the protoplanetary disk (Madhusudhan 2012a; Ali-Dib et al. 2014; Madhusudhan et al. 2014; Thiabaud et al. 2015). Many C/O ratios were measured for transiting planets along with studies to explain some of the higher ratios (i.e., Madhusudhan et al. 2011a; Madhusudhan 2012a,b; Moses et al. 2013; Teske et al. 2013b,a; Line et al. 2014). Directly imaged companions also started to have their C/O ratios measured, with the hope that these youthful systems would not have undergone significant chemical evolution (Konopacky et al. 2013; Wilcomb et al. 2020; Mollière et al. 2020; Petrus et al. 2021; Zhang et al. 2021; Ruffio et al. 2021; Hoch et al. 2022; Palma-Bifani et al. 2022). The C/O ratio measurement may be able to trace the formation location of these objects and how they collected gas and solids in their evolving protoplanetary disks (Öberg et al. 2011; Madhusudhan et al. 2017; Mordasini et al. 2016; Booth et al. 2017; Cridland et al. 2019; Eistrup et al. 2018). More recently, Mollière

et al. (2022) conducted a study using state-of-the-art formation models, including the chemical evolution of the protoplanetary disk, showing that chemical abundance measurements are crucial for informing new formation models.

Spectral characterization of exoplanets and substellar companions can shed light on how they may have formed. The current directly imaged companions are young (< 200 Myr), and thus their atmospheres have not undergone extensive post-formation chemical evolution and could point towards how and where they formed in the protoplanetary disk. In contrast, the transiting Hot Jupiters are typically older and have gone through significant chemical evolution. Still, atmospheric composition measurements may provide hints about their formation.

Here, we present a statistical analysis of the C/O ratio formation tracer using compiled values from directly imaged companions and a sample of transit/eclipse companions. In Section 2, we report the C/O ratios used for this work and how they were measured. In Section 3, we report our observations of HD 284149 AB b, data reduction methods, atmospheric modeling, C/O ratio measurement, and non-detections of two targets with the OSIRIS instrument on the W.M. Keck Telescope. In section 3.6 we measure dynamical masses for HD 284149 AB b and HD 284149 B. In Section 4 we compare C/O ratios of 25 transiting and eclipsing planets from Changeat et al. (2022) to C/O ratios of the directly imaged planets. We find a trend between C/O ratio and companion mass and compute two metrics to determine if the planets originate from the same underlying population. In Section 5 we discuss the implications of our results and in Section 6 we discuss our conclusions and future work.

2. C/O RATIO MEASUREMENTS FROM THE LITERATURE

2.1. Direct Imaging Spectroscopy

Direct imaging spectroscopy has allowed for the C/O ratio measurements of many imaged substellar companions. Here we review the current suite of C/O ratios derived for directly imaged planets. Lee et al. (2013) ran a retrieval on low-resolution spectral data and photometric points on HR 8799 b from Barman et al. (2011), Currie et al. (2011), Skemer et al. (2012), and Galicher et al. (2011) resulting in C/O ratios that were approximately unity across their various models. Lavie et al. (2017) created an open source code HELIOS-RETRIEVAL and ran this code on the HR 8799 planets using data from Zurlo et al. (2016), Ingraham et al. (2014), Barman et al. (2011), and Barman et al. (2015). They estimated C/O

values that ranged from superstellar for HR 8799 b to consistent with stellar for HR 8799 c and substellar for HR 8799 d and e. [Mollière et al. \(2020\)](#) derived a C/O ratio of $0.60^{+0.07}_{-0.08}$ for HR 8799 e through atmospheric retrievals using their code *petitRADTRANS* ([Mollière et al. 2019](#)) with the added effect of multiple scattering to better treat cloudy objects. They ran retrievals on *K*-band GRAVITY data ([Gravity Collaboration et al. 2017](#)) and archival SPHERE and GPI data. [GRAVITY Collaboration et al. \(2020\)](#) measured C/O ratios for β Pic b using forward modeling with the newest ExoREM grid [Charnay et al. \(2018\)](#) (0.43 ± 0.05) and retrievals with *petitRADTRANS* ($0.43^{+0.04}_{-0.03}$) on *K*-band GRAVITY spectra and GPI *Y-J-H*-band spectra. [Petrus et al. \(2021\)](#) calculated an upper limit for the C/O ratio of HIP 65426 b to be ≤ 0.55 using a Bayesian inference with BT-Settl with the ForMoSA code on SINFONI medium-resolution *K*-band data ([Petrus et al. 2020](#)). A C/O ratio for TYC 8998-760-1 b (YSES-1 b) was derived to be $0.52^{+0.04}_{-0.03}$ by [Zhang et al. \(2021\)](#) using Bayesian retrieval analysis on SINFONI medium-resolution *K*-band data with *petitRADTRANS*. [Palma-Bifani et al. \(2022\)](#) forward modeled *J*-, *H*-, and *K*-band SINFONI data of AB Pic b using ExoREM and BT-SETTL13 atmospheric models and the ForMoSA forward modeling code to obtain a C/O ratio of 0.58 ± 0.08 . [Brown-Sevilla et al. \(2023\)](#) re-reduced SPHERE data on 51 Eri b and performed a retrieval using *petitRADTRANS* on low-resolution *Y-H* spectrum and revised K1-K2 photometry to obtain a C/O ratio of 0.38 ± 0.09 . [Wang et al. \(2023\)](#) performed an atmospheric retrieval on HR 8799 c photometric data along with low- and high-resolution spectroscopic data ($R \sim 20\text{-}35,000$) and obtained a C/O ratio of $0.67^{+0.12}_{-0.15}$.

Our team has derived C/O ratios for six directly imaged companions using the OSIRIS IFU. C/O ratios for the three HR 8799 planets, HR 8799 b, c, and d were derived by [Ruffio et al. \(2021\)](#) to be $0.578^{+0.004}_{-0.005}$, 0.562 ± 0.004 , and $0.551^{+0.005}_{-0.004}$ respectively quoting statistical uncertainties. Notably, our values for the HR 8799 planets are consistent with those from other high-resolution spectra ([Wang et al. 2023](#)), but not with all those derived from retrievals of low-resolution spectra. When using the values in [Ruffio et al. \(2021\)](#) we adopt the C/O uncertainties calculated in previous measurements by [Konopacky et al. \(2013\)](#) of 0.1 instead, because these measurements are dominated by model uncertainties that are not captured during the fitting process. [Ruffio et al. \(2021\)](#) used a custom *PHOENIX* model grid and a forward modeling approach on OSIRIS IFU data to derive these ratios. [Wilcomb et al. \(2020\)](#) derived the C/O ratio for κ And b to be $0.704^{+0.09}_{-0.24}$ follow-

ing a forward modeling approach on the OSIRIS data using a custom *PHOENIX* model grid. We measured VHS 1256 b’s C/O ratio as $0.590^{+0.28}_{-0.354}$ in [Hoch et al. \(2022\)](#) following the same approach as [Wilcomb et al. \(2020\)](#) using custom *PHOENIX* models that included a cloud parameter to treat the thick clouds of an “L/T” transition object. [Petrus et al. \(2023\)](#) measured the upper limit of the C/O ratio for VHS 1256 b to be > 0.63 , which is encompassed in the error bars in [Hoch et al. \(2022\)](#).

2.2. Transit/Eclipse Spectroscopy

Transiting exoplanets can occasionally offer low- to high-resolution spectra that can, in turn, allow for the derivation of atmospheric properties such as the C/O ratio. Low-resolution data cannot reveal individual spectral lines, unlike moderate resolution data, so retrievals are often used to derive these properties. [Changeat et al. \(2022\)](#) reanalyzed HST WFC3 G141 Grism data using their pipeline, *Iraclis* ([Tsiaras et al. 2016](#)), and Spitzer data of 25 Hot Jupiters. The retrieval code used was *Alfnoor* ([Changeat et al. 2020](#)), and the equilibrium chemistry retrievals were conducted using the GGChem code ([Woitke et al. 2018](#)). Furthermore, [Changeat et al. \(2022\)](#) used the two retrieval methods on both HST and Spitzer data and on them individually to obtain C/O ratio measurements for all 25 exoplanets in their sample. Some high-resolution spectra of transiting planets have been obtained using instruments such as CFHT/SPIRou, Keck/KPIC, and GG/IGRINS to better constrain the C/O ratio and individual chemical abundances of Hot Jupiters ([Boucher et al. 2023](#); [Finnerty et al. 2023](#); [Pelletier et al. 2021](#); [Line et al. 2021](#)).

2.3. System Parameter Compilation

We chose to use C/O ratio values obtained using moderate- high-resolution data for the directly imaged companions. The inconsistency of the moderate/high resolution C/O values with those from low resolution retrievals is something of a conundrum. However, the ability to resolve spectral lines in higher resolution data is advantageous. There are instances of retrievals returning C/O ratios near unity that are highly inconsistent with the moderate resolution spectra, which would show different spectral lines near $C/O \sim 1$. Therefore, we choose to use results from data where spectral lines are resolved. This results in not all directly imaged planets with C/O estimates described in the previous section being included in our analysis below, but we believe offers a sample that is the most consistent. For the most part only low resolution data is available for transiting

planets, and so our goal for this population is uniformity in approach and analysis. We therefore adopt the C/O ratios from [Changeat et al. \(2022\)](#), which presents a uniform sample and analysis of transiting Hot Jupiters.

We compiled various parameters of both the directly imaged and transiting systems, choosing the most recent reported values, such as projected separation (au), companion mass (M_{Jup}), host star mass (M_{\odot}), and age (Myr) in addition to C/O ratios of the respective planets. For the directly imaged planets, we used dynamical masses when there were measurements available. For the transiting planets, we used values computed by [Changeat et al. \(2022\)](#). In particular, we chose [Changeat et al. \(2022\)](#) C/O ratio values that were derived through equilibrium chemistry retrieval (eq) on the combination of Spitzer and HST data. If the object did not have a measurement from the retrieval on both data-sets, we chose the HST-data only measurement from the equilibrium retrieval. This provided us with two populations, directly imaged planets and transit/eclipse planets, with derived C/O ratios that we could conduct a population comparison. Our compiled values are presented in Table 3. We chose the values from [Changeat et al. \(2022\)](#) because they were all analyzed in the same way, by the same code, rather than obtaining values from literature that may be plagued with different systematics.

3. ADDITIONAL DATA FROM OSIRIS

As described in the previous section, a significant number of the sources with C/O ratios compiled here come from our previous work on OSIRIS ([Barman et al. 2015](#); [Konopacky et al. 2013](#); [Ruffio et al. 2021](#); [Wilcomb et al. 2020](#); [Hoch et al. 2022](#)). Here we report on one additional observation that we add to the full list of sources. We also describe two non-detections in our OSIRIS survey.

3.1. Target Information

HD 284149 AB b is a substellar companion orbiting at $\sim 3.6''$ from the F8 star HD 284149 A and a stellar companion HD 284149 AB b discovered by [Bonavita et al. \(2014, 2017\)](#). The HD 284149 system has been proposed to be a part of the Taurus-Ext association ([Luhman et al. 2017](#); [Kraus et al. 2017](#); [Daemgen et al. 2015](#)) with an age estimate by [Bonavita et al. \(2014\)](#) of 25_{-10}^{+25} Myr. [Bonavita et al. \(2017\)](#) found an effective temperature of 2395 ± 113 K, a spectral type of $M9 \pm 1$, and a mass of $26 \pm 3 M_{\text{Jup}}$ for the substellar companion HD 284149 AB b. We calculate dynamical masses for components of the HD 284149 system that provide updated model-independent mass values of $170_{-16}^{+23} M_{\text{Jup}}$ (or $0.16 \pm 0.02 M_{\odot}$) and $28.26_{-1.0}^{+0.75} M_{\text{Jup}}$ HD 284148 B

and HD 284149 AB b respectively as described in Section 3.6.

3.2. Data Reduction

HD 284149 AB b was observed on 2017 November 3 with the OSIRIS integral field spectrograph (IFS, [Larkin et al. 2006](#)) on the W.M. Keck I telescope. We used the K broadband mode (1.965–2.381 μm) with a spatial sampling of 20 milliarcseconds per lenslet. We integrated on the object for 50 minutes via 5 exposures of 10 minutes each, where we dithered up and down by a 2-3 pixels between exposures. Observations of a blank patch of sky and of our A0V telluric standard (HIP 16095) were obtained close in time with the object data. We also obtained dark frames with exposure times matching our dataset. The data were reduced using the OSIRIS data reduction pipeline (DRP; [Krabbe et al. 2004](#); [Lockhart et al. 2019](#)). Data cubes (x, y, λ) were generated using the OSIRIS DRP with rectification matrices provided by the observatory for the correct time frame of the observations. At the advice of the DRP working group, we did not use the Clean Cosmic Rays DRP module (T. Do, priv. comm) and we did not use scaled sky subtraction. An example data cube image frame is shown in Figure 1.

Once the one-dimensional spectra for the telluric sources were extracted, we used the DRP to remove hydrogen lines, divide by a blackbody spectrum of the appropriate temperature, and combine all standard star spectra. The individual telluric spectra were median combined and produced a telluric calibrator spectrum. The telluric correction for HD 284149 AB b was then completed by dividing the final telluric calibrator spectrum from all object frames.

Once the object data cubes are fully reduced, we identify the location of the target. When conducting high contrast observations with OSIRIS, the location of a companion can be challenging to find due to the brightness of the speckles from the host star. For HD 284149 AB b, the separation from the host star is wide enough and the companion is bright enough that the speckles from the host star do not impact the spectrum of the companion, and identification is straightforward (see Figure 1).

We extract the object spectrum from the data cubes using a box of 3×3 spatial pixels (spaxels). Once we extracted the HD 284149 AB b spectra from each frame for all data cubes, we then normalize each individual spectrum to account for PSF and background fluctuations. Finally, we median-combine all 5 individual spectra, and do a barycentric correction on the individual spectra. To calibrate the flux of our spectra we calculated the flux



Figure 1. An example data cube image, collapsed in wavelength via median, from our OSIRIS HD 284149 AB b dataset. The field of view is $0.32'' \times 1.28''$. The bright spot shows the companion clearly visible without any need for speckle removal.

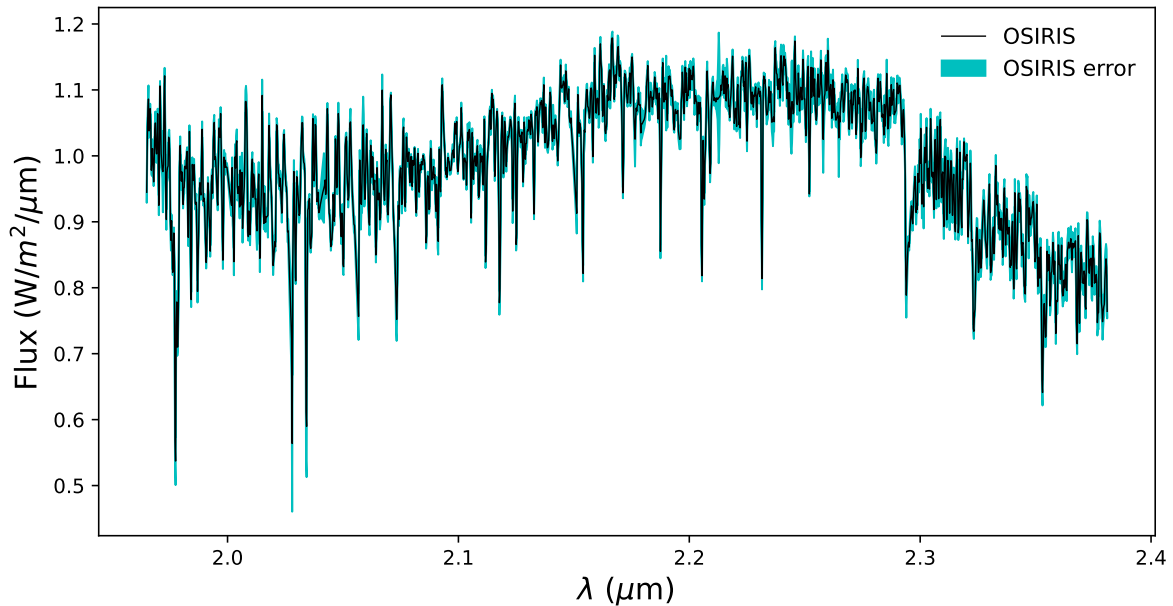


Figure 2. Our fully reduced, combined, and flux calibrated, moderate-resolution OSIRIS *K*-band spectra of HD 284149 AB b. The errors are calculated from the RMS of the individual spectra at each wavelength. The error includes uncertainties in both the continuum and the lines. The total spectral uncertainties are represented as a shaded blue region. The CO bandhead is distinctly visible at $2.3 \mu\text{m}$.

at each wavelength such that, when integrated, the flux matches the most recent K -band apparent magnitude (14.332 ± 0.04) from Bonavita et al. (2014).

Uncertainties were calculated by determining the RMS between the individual spectra at each wavelength. These uncertainties include contributions from statistical error in the flux of the planet and the molecular lines. The OH sky lines are subtracted extremely well and have a negligible contribution to the uncertainties. The final combined and flux calibrated spectrum is shown in Figure 2.

Narrow spectral features are more easily analyzed by removing the continuum because we can avoid low spatial frequency errors (from residual and/or faint speckles) that affect the continuum shape. We remove the continuum from our fully reduced and flux calibrated spectra using a similar continuum removal process we have used in the past for OSIRIS data (e.g., Barman et al. 2015; Wilcomb et al. 2020; Hoch et al. 2022). To remove the continuum, we employ a high-pass filter with a kernel size of 200 spectral bins to each of the individual spectra. We then subtract the smoothed spectrum without spectral lines from the original spectra. Once all the individual spectra are flattened, we median combine them using the method for the continuum spectra and find the uncertainties by determining the RMS of the individual spectra at each wavelength.

3.3. Spectral Modeling

To determine the effective temperature (T_{eff}), surface gravity ($\log g$), and metallicity ($[M/H]$) of HD 284149 AB b we used the *PHOENIX* model-based Göttingen spectral library (Husser et al. 2013). We chose to use the Göttingen spectral library because they are *PHOENIX* models that cover the estimated temperature and surface gravity of HD 284149 AB b from previous studies, and therefore there was no need to create additional custom *PHOENIX* models.

Here, we use a forward-modeling process following Blake et al. (2010), Burgasser et al. (2016), Hsu et al. (2021b), and Theissen et al. (2022) to determine the best-fit model from the grid. The effective temperature (T_{eff}), surface gravity ($\log g$), and metallicity ($[M/H]$) are inferred using a Markov Chain Monte Carlo (MCMC) method built on the *emcee* package that uses an implementation of the affine-invariant ensemble sampler (Goodman & Weare 2010; Foreman-Mackey et al. 2013). Our MCMC runs used 100 walkers, 500 steps, and a burn-in of 400 steps to ensure parameters were well mixed, and the description of the MCMC calculations are described in Wilcomb et al. (2020).

The results show that HD 284149 AB b has a super-solar metallicity. D’Orazi et al. (2011) derived that the Taurus-Auriga association has a mean solar metallicity ($[Fe/H] = -0.01 \pm 0.05$). If this value is adopted for the Taurus-Ext association, the substellar companion is enhanced comparatively. The best fit parameters from our continuum K -band OSIRIS data are $T_{\text{eff}} = 2502_{-11}^{+19}$ K, $\log g = 4.52_{-0.14}^{+0.22}$, and $[M/H] = 0.37_{-0.12}^{+0.18}$. The temperature results are in good agreement with the temperature from Bonavita et al. (2017), which was 2395 ± 113 K. Figures 3–4 show the best-fit model for the continuum data and the corresponding corner plot from our MCMC analysis. We note that there are several lines that appear to be stronger in the data than in the model in Figure 3. We have verified that these are not residual telluric contamination, but instead real lines, likely from scandium, yttrium, titanium, and iron. We note that stronger lines in the data than the *PHOENIX* models is a known phenomenon for scandium, yttrium, and titanium in high-metallicity, low temperature objects. It is due to the stronger impact of non-LTE effects on these lines due to hyperfine splitting (e.g., Bergemann et al. 2012; Thorsbro et al. 2018). Since our focus in this work is carbon and oxygen, and the mismatch of these lines will not change the derived effective temperature or $\log(g)$, which are strongly dependent on the continuum shape and CO lines, we do not attempt further modeling of these lines. Given the good signal-to-noise ratio of this spectrum, potential future work could involve detailed modeling of these lines to obtain precise abundances for these elements.

We then ran our fitting procedure on the continuum subtracted data using the same grid. We employed the same filtering code used to flatten the data on the model grid to flatten the models. The best fit parameters from our continuum subtracted K -band OSIRIS data are $T_{\text{eff}} = 2605_{-13}^{+19}$ K, $\log g = 4.91_{-0.074}^{+0.060}$, and $[M/H] = 0.11_{-0.067}^{+0.076}$. Figures 5–6 show the best-fit model for the continuum subtracted data and the corresponding corner plot from our MCMC analysis. Our continuum subtracted results are similar to our continuum results, but are not consistent within the error bars. In order to encompass the results from both fits, we adopt values of $T_{\text{eff}} = 2502$ K, with a range of 2291–2624 K, $\log g = 4.52$, with a range of 4.38–4.91, and $[M/H] = 0.37$, with a range of 0.10–0.55 summarized in Table 1.

3.4. C and O Abundances

With best fit values for temperature, surface gravity, and metallicity, we can derive abundances of C and O using our OSIRIS K -band spectra. We chose the best-fit values from the continuum fits of the data because the

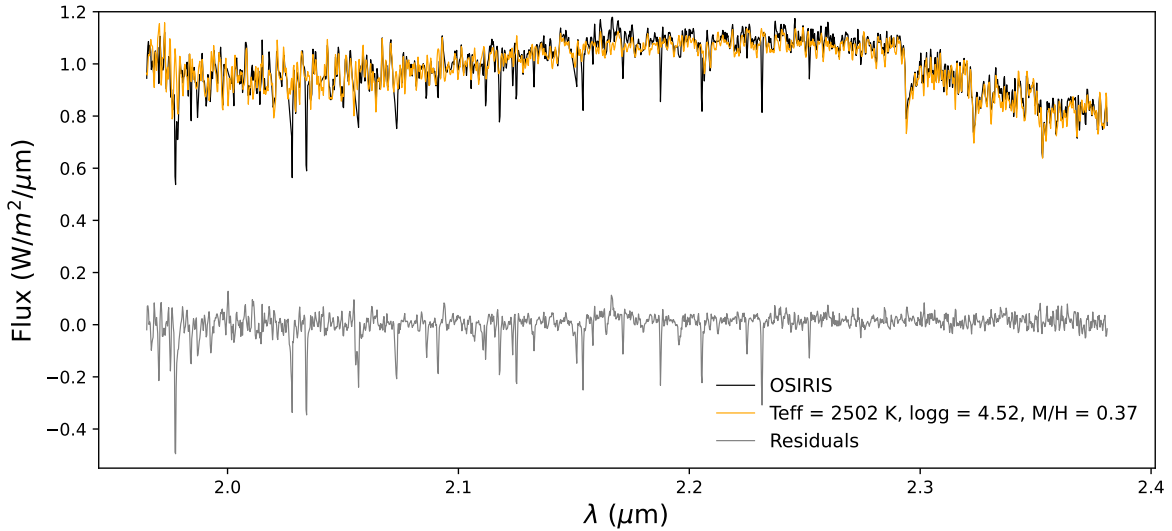


Figure 3. Our fully reduced, combined, and flux calibrated moderate-resolution OSIRIS *K*-band spectra of HD 284149 AB b in black plotted against the best-fit model in orange. The residuals are plotted below in gray.

Table 1. Summary of atmospheric parameters derived from MCMC fits.

Spectra	Effective Temperature	Surface Gravity	Metallicity
HD 284149 AB b	T_{eff} (K)	$\log g$	[M/H]
PHOENIX-ACES			
OSIRIS Including Continuum	2502^{+19}_{-11}	$4.52^{+0.22}_{-0.14}$	$0.37^{+0.18}_{-0.12}$
OSIRIS Continuum Subtracted	2605^{+19}_{-13}	$4.91^{+0.060}_{-0.074}$	$0.11^{+0.076}_{-0.067}$
Adopted Values	2502	4.52	0.37
Allowed Range of Values	2291–2624	4.38–4.91	0.10–0.55

[–]Based on our fitting, we have chosen to adopt the best-fit values from the Göttingen spectral library fit to the OSIRIS data with the continuum included. However, we allow for uncertainties that encompass the range of most fits to both the continuum data and the continuum subtracted data.

the results from either fit were fairly similar, and the continuum contains important information about the temperature when not biased by speckles, as is the case here. We constructed a mini-grid using *PHOENIX* that holds our derived parameters the same, but varies the abundance of C and O. C and O were each varied from 0 to 1000 times Solar using a uniform logarithmic sampling, resulting in 12 synthetic spectra. We fit for the abundance of C first, holding O at its initial value. Next, the C abundance was set to its nominal value, and we fit for O. We choose not to vary the bulk atmospheric parameters (temperature, $\log(g)$, and metallicity) in this grid because they are constrained by the continuum. A change in C or O abundance will not change the shape of the continuum to result in an improved fit, but will instead impact line depths. While the depths of the lines

are impacted by bulk parameters, it would not be possible to jointly improve the continuum and the line depths by only varying the C and O abundance. Indeed, this effect was seen in [Konopacky et al. \(2013\)](#), where a grid with variation in temperature, gravity, and C and O was used but all best fits were at the same temperature and gravity as determined using the continuum information.

Figure 7 shows the resulting χ^2 distribution as a function of C and O abundance. The models with the lowest χ^2 when compared to the flattened data gave us the best-fits for both C and O. The best fit for C had an abundance scaling of $1.00^{+0.30}_{-0.45}$, and the best fit for O had a lower limit abundance scaling of solar or $1.00^{+0.37}_{-0.03}$. To calculate the 1- σ uncertainties in each mole fraction value, we used the values from models within ± 1 of our lowest χ^2 .

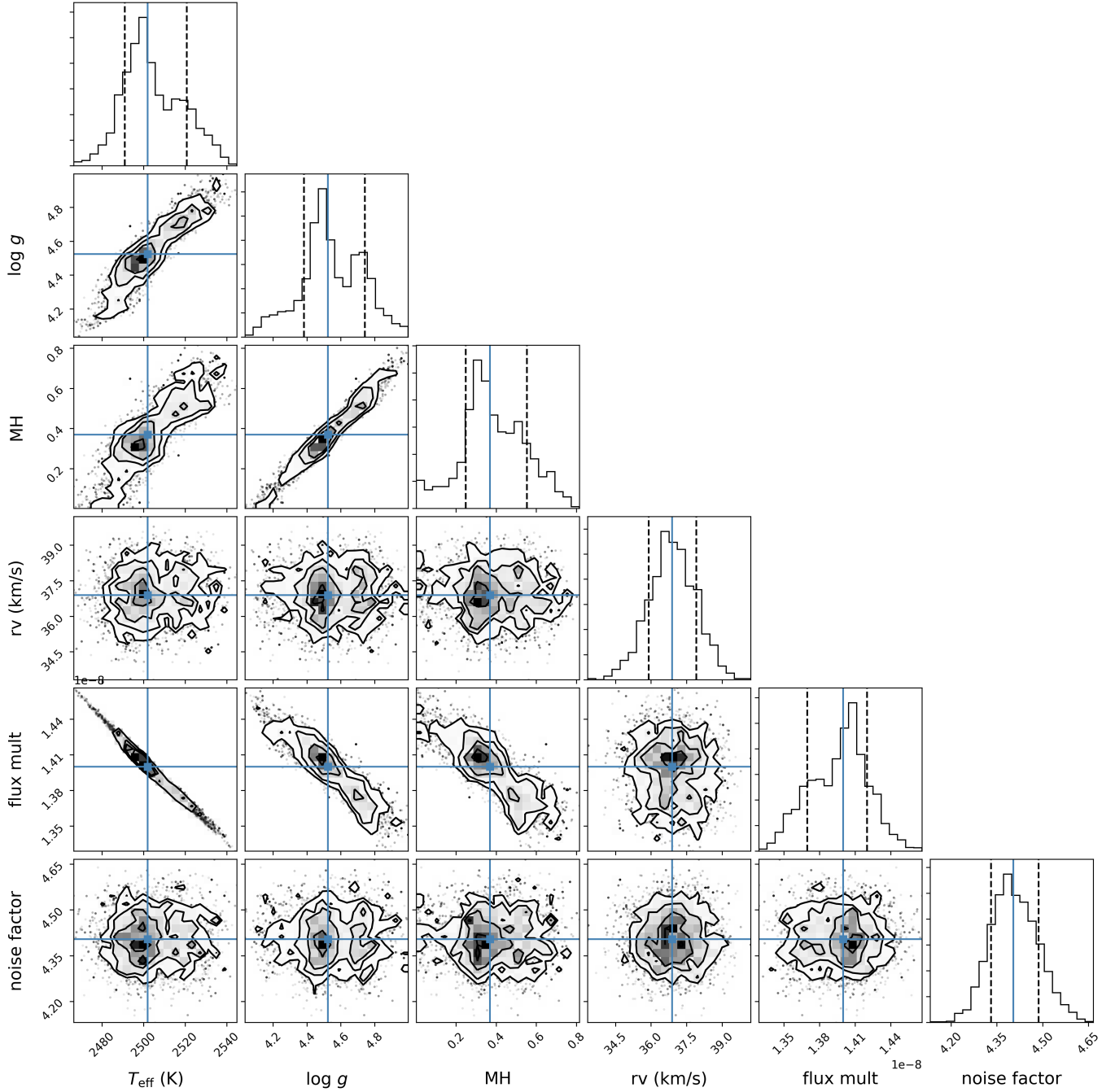


Figure 4. Corner plot from our MCMC fits for our continuum OSIRIS *K*-band spectra. The diagonal shows the marginalized posteriors. The covariances between all the parameters are in the corresponding 2-d histograms. The blue lines represent the 50th percentile, and the dotted lines represent the 16 and 84 percentiles. The “flux mult” corresponds to the dilution factor that scales the model by $(radius)^2(distance)^{-2}$.

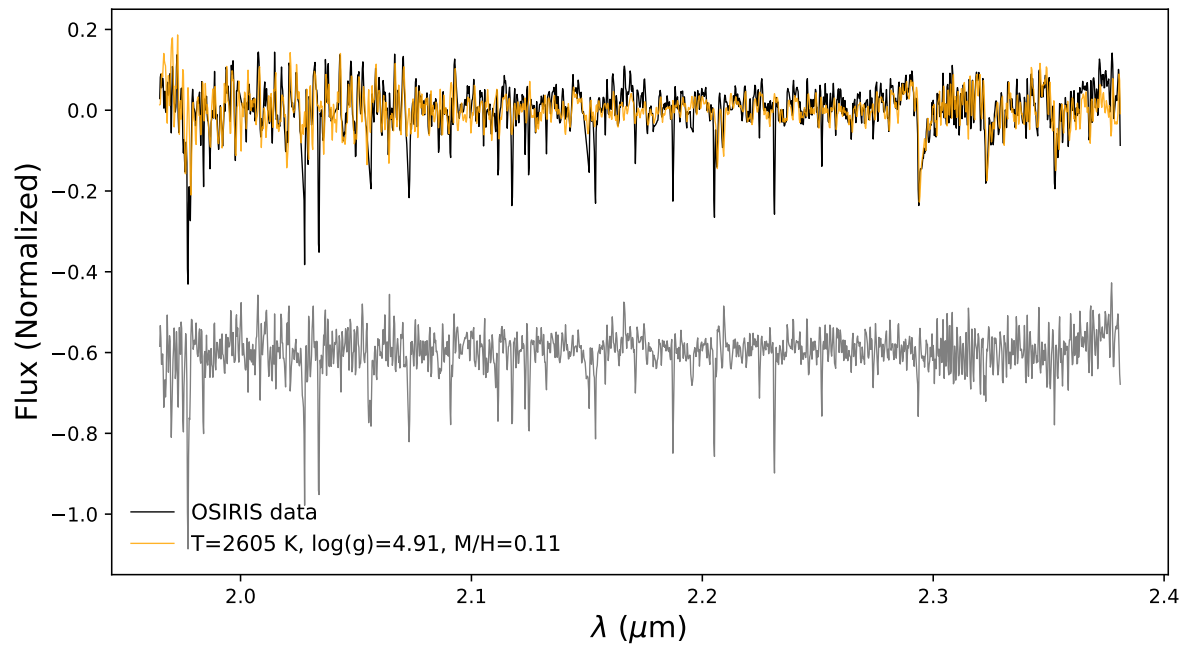


Figure 5. Our fully reduced, combined, and continuum subtracted moderate resolution OSIRIS *K*-band spectra of HD 284149 AB b in black plotted against the best-fit model in orange. The residuals are plotted below in gray.

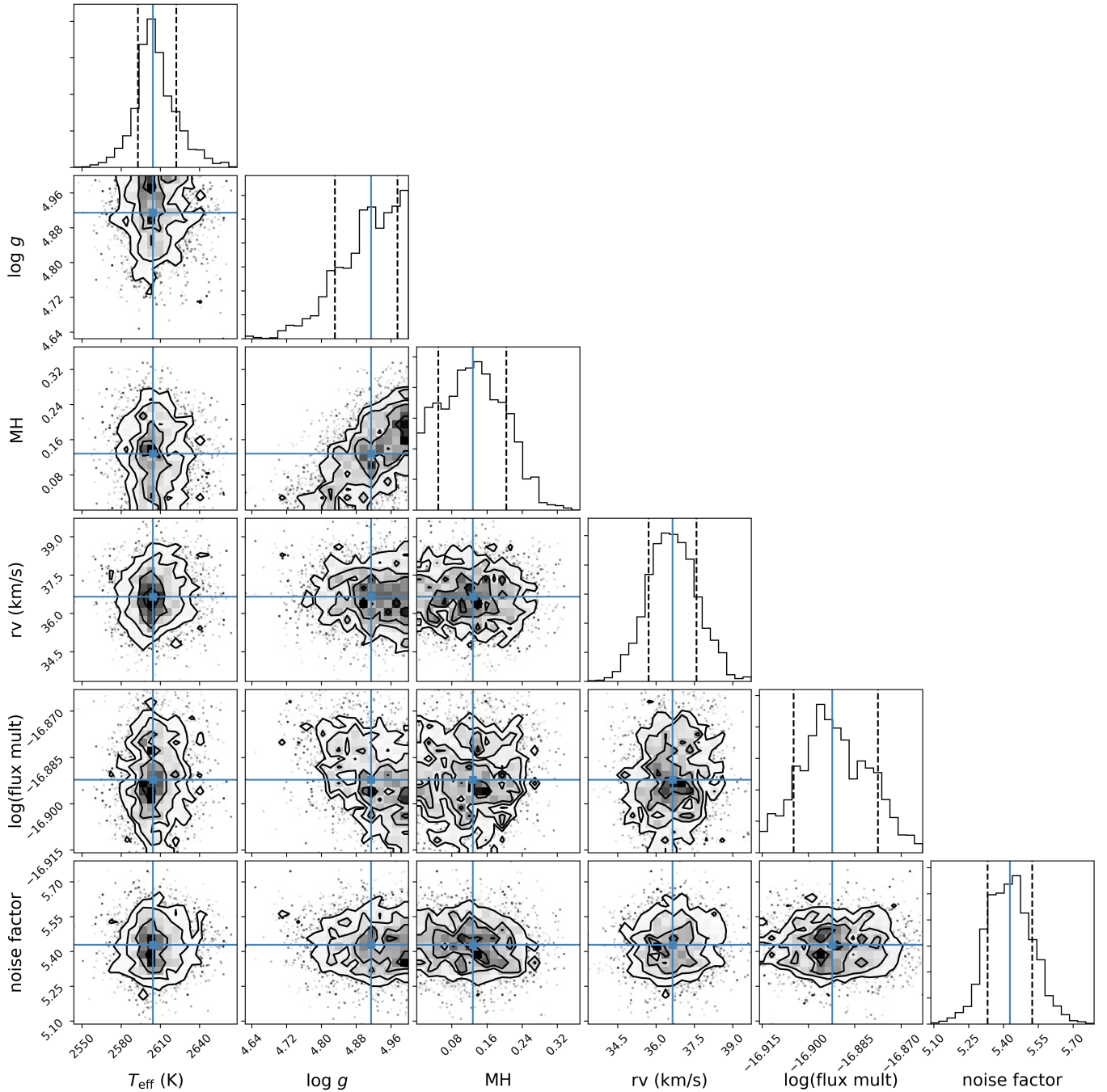


Figure 6. Corner plot from our MCMC fits for our continuum subtracted OSIRIS K -band spectra.

3.5. C/O Ratio for HD 284149 AB b

In our previous work, we have used OSIRIS data to constrain the C/O ratios of directly imaged companions such as HR 8799 b, c, and d, κ Andromedae b and VHS 1256 b (e.g., Konopacky et al. 2013; Wilcomb et al. 2020; Ruffio et al. 2021; Hoch et al. 2022). For giant planets formed by rapid gravitational instabilities, their atmospheres should have elemental abundances that are similar to their host stars (Helled & Schubert 2009).

If giant planets form by a core/pebble accretion process, there could be a range of elemental abundances possible (Öberg et al. 2011; Madhusudhan 2019). In this framework, the abundances of giant planets' atmospheres formed by core/pebble accretion are highly dependent on the location of formation relative to CO , CO_2 , and H_2O frost lines and the amount of solids collected during runaway accretion phase. This can potentially be diagnosed using the C/O ratio.

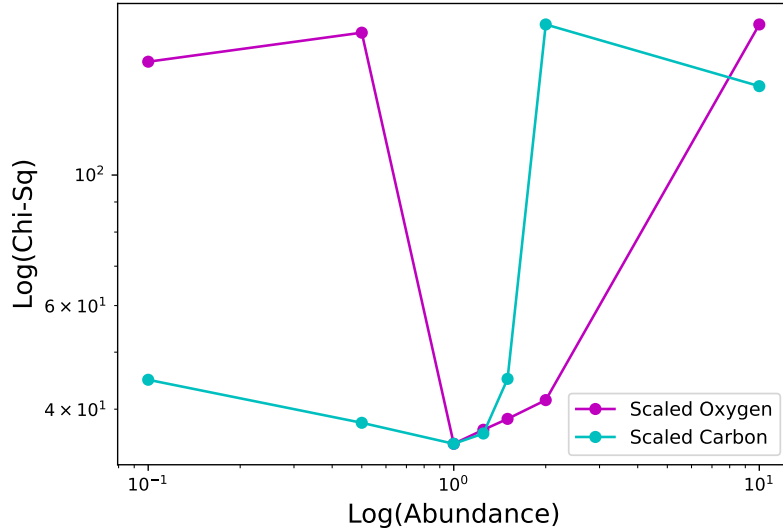


Figure 7. Results of $T_{\text{eff}} = 2502_{-11}^{+19}$ K, $\log g = 4.52_{-0.14}^{+0.22}$, and $[M/H] = 0.37_{-0.12}^{+0.18}$ model fits with varying abundances for both C and O to our continuum-subtracted OSIRIS spectrum. The abundances are given in units relative to the ratio in the Sun, such that a value of zero implies the solar value. The scalings of C prefer solar as well as the scalings of O prefer solar values. From these fits we find $C/O = 0.59_{-0.30}^{+0.15}$.

The C/O ratio is dependent on the abundances of C and O in the atmosphere. The equation used for this derivation is

$$\frac{C}{O} = 10^{\epsilon_C - \epsilon_O},$$

where ϵ is the scaled abundance relative to Solar. The C/O ratio we derive for HD 284149 AB b is $0.59_{-0.30}^{+0.15}$.

3.6. Dynamical Masses of the HD 284149 System

Previous calculations of mass values of the HD 284149 system calculated by Bonavita et al. (2017) are derived from the measured photometry of the stellar and substellar components. The adopted mass values in Bonavita et al. (2017) are $0.16 \pm 0.04 M_{\odot}$ for HD 284149 B and $26 \pm 3 M_{\text{Jup}}$ for HD 284149 AB b. Photometric mass values are inherently dependent on the stellar age, which can drive large uncertainties, or sometimes even discrepancies, between the derived photometric model-dependent mass and the dynamical model-independent mass. Model-independent dynamical masses of stellar and substellar companions, that do not depend on a stellar age estimate, can be determined from orbital information. In particular, combining astrometric accelerations from Hipparcos (Perryman et al. 1997) and Gaia eDR3 (Gaia Collaboration et al. 2021) with measured relative astrometry from direct imaging as demonstrated in Rickman et al. (2022) has been shown to be a powerful way to estimate companion masses.

We have calculated preliminary dynamical masses of HD 284149 B and HD 284149 AB b using the astrometric accelerations from the Hipparcos-Gaia catalog of accelerations (HGCA; Brandt 2021) and the relative astrometry from Bonavita et al. (2017). This astrometric information can be combined using orvara (Brandt et al. 2021) which is an orbit-fitting code specifically designed to combine absolute astrometric data from Hipparcos and Gaia, with relative astrometry from direct imaging that has the capability of fitting multi-planet systems.

We ran the MCMC orbital fit with 500,000 steps in each chain for both HD 284149 AB b and HD 284149 B, with a prior set on the mass of the primary star HD 284149 A of $1.14 \pm 0.05 M_{\odot}$ (Bonavita et al. 2014). The resulting orbital plots are shown in Figure 8 and the fits to the astrometric accelerations are shown in Figure 9, with the corner plots for HD 284149 B and HD 284149 AB b are shown in Figure 10 and Figure 11 respectively.

Using this approach we derive a dynamical mass of the inner companion HD 284149 B of $M = 170_{-16}^{+23} M_{\text{Jup}}$ (or $0.16 \pm 0.02 M_{\odot}$) which is in agreement with the photometric value derived in Bonavita et al. (2017) of $0.16 \pm 0.04 M_{\odot}$. We also derive a dynamical mass of the substellar companion HD 284149 AB b of $M = 28.26_{-1.00}^{+0.75} M_{\text{Jup}}$, which is also in agreement with the photometrically-derived mass of $26 \pm 3 M_{\text{Jup}}$ from Bonavita et al. (2017). The close correspondence of the dynamical mass estimate and the photometrically-

derived mass is encouraging, and provides additional weight to the estimated age of the system.

We note that in spite of the small error bars on the derived mass, there might be biases in this result due to low phase coverage of astrometry for this orbit. Even with the long time baseline of Hipparcos and Gaia, the estimated orbital period of ~ 7300 years for the companion means that the orbit phase coverage is only 0.3%. Minimal orbit coverage can result in biases in the resulting orbital parameters (e.g., Kosmo O’Neil et al. 2019; Ferrer-Chávez et al. 2021; Do Ó et al. 2023), particularly when there are systematics in the astrometric data that are not accounted for. It is outside the scope of this paper to explore the orbital properties and astrometry of this system in detail, but we take the derivation of a similar dynamical mass to the photometric mass as an indication that using the current system age estimate is reasonable. Therefore, we use the photometrically derived mass of HD 284149 AB b in our C/O ratio analysis in Section 4.

3.7. Non-Detections

For our imaging spectroscopy survey of exoplanetary atmospheres with Keck/OSIRIS we have thus far gathered K -band data on eight directly imaged planets; κ And b, VHS 1256 b, HR 8799 bcd, HD 284149 AB b, GJ 504 b, and 51 Eri b. GJ 504 b and 51 Eri b were not detected in our OSIRIS data and details of the observations are in Table 2. GJ 504 b is a Jovian planet of $4_{-1.0}^{+4.5} M_{\text{Jup}}$ orbiting at a projected separation of 43.5 au around the Sun-like G0-type star, GJ 504 (Kuzuhara et al. 2013). GJ 504 b is significantly cooler than other imaged exoplanets with an effective temperature of about 510_{-20}^{+30} K. GJ 504 b is also the first directly imaged planet around a metal-rich host star. 51 Eri b is a gas giant planet that was discovered orbiting the ~ 20 Myr 51 Eridani star at 13 au (Macintosh et al. 2015). 51 Eri b is about 600-750 K with a mass of about $2\text{--}12 M_{\text{Jup}}$. Both of these planets are lower temperature and lower mass than the majority of the directly imaged companions, and would be excellent candidates for atmospheric characterization to compare to their hotter counterparts.

For GJ 504 b, we conducted observations in the K broadband mode (1.965–2.381 μm) with a spatial sampling of 0.050'' per lenslet for this object with the hope of enhancing its detectability via coarser spatial sampling. We observed a telluric calibrator star (HIP 65599) and obtained sky frames in close time to observations of the object. Data cubes (x, y, λ) were generated after operating the OSIRIS DRP using the observatory provided rectification matrices for the same time frame of the ob-

servations, following the steps described in section 4.2. After reduction and telluric correction, we tried to locate the planet in the data cubes. The separation of GJ 504b means that the speckles were not as bright as some of our other targets, so our attempt to locate the planet was primarily without any speckle removal. We did not see a clear signal when looking at the data-cubes. We then tried a cross-correlation approach using a *PHOENIX* model of similar atmospheric parameters (Ruffio et al. (2019)) and still did not see a clear signal in our OSIRIS data.

For 51 Eri b, we conducted observations in the K broadband mode (1.965–2.381 μm) with a spatial sampling of 0.020'' per lenslet, observed a telluric standard star (HIP 25453) and sky frames in close time to object observations. Data cubes were generated using the OSIRIS DRP as with the other sources. We did not see a clear signal in the raw data, and we also tried a cross-correlation approach using a *PHOENIX* model of similar atmospheric parameters and did not detect the planet. Given that the detections of these targets is currently beyond what we can achieve with OSIRIS, both GJ 504 b and 51 Eri b would be great candidates for JWST and upcoming extremely large telescopes (ELTs) that may have better sensitivity to objects of high contrast and/or low temperature.

4. C/O RATIO ANALYSIS

Table 3 shows all compiled values of C/O ratio for both transiting and directly imaged planets, including our new addition of HD 284149 AB b. Other system parameters are included as well. We explored C/O versus each of those parameters, noting whether the measurements are with transit or direct spectroscopy. The results of this analysis are shown in Figures 12–15. We see a trend when plotting companion mass against C/O ratio, shown in Figure 12. All companions that are above $3\text{--}5 M_{\text{Jup}}$ have C/O ratios around 0.7 ± 0.2 , and companions with masses less than $3\text{--}5 M_{\text{Jup}}$ exhibit a wider spread, with C/O ratios of up to 1.6.

To verify this distinction in C/O ratio around $3\text{--}5 M_{\text{Jup}}$, we performed a few statistical tests. We conducted a Kolmogorov–Smirnov Test (KS Test), and an Anderson-Darling Test (AD Test) because they are well-established tests of similarity to determine if two distributions come from the same parent distribution. We first randomly sampled 100,000 values from each parameter (C/O ratio and companion mass) using a Gaussian distribution centered on the central value with a width defined by the uncertainty. For non-symmetric error bars we used a triangle function, centered on the central value with two widths of upper and lower er-

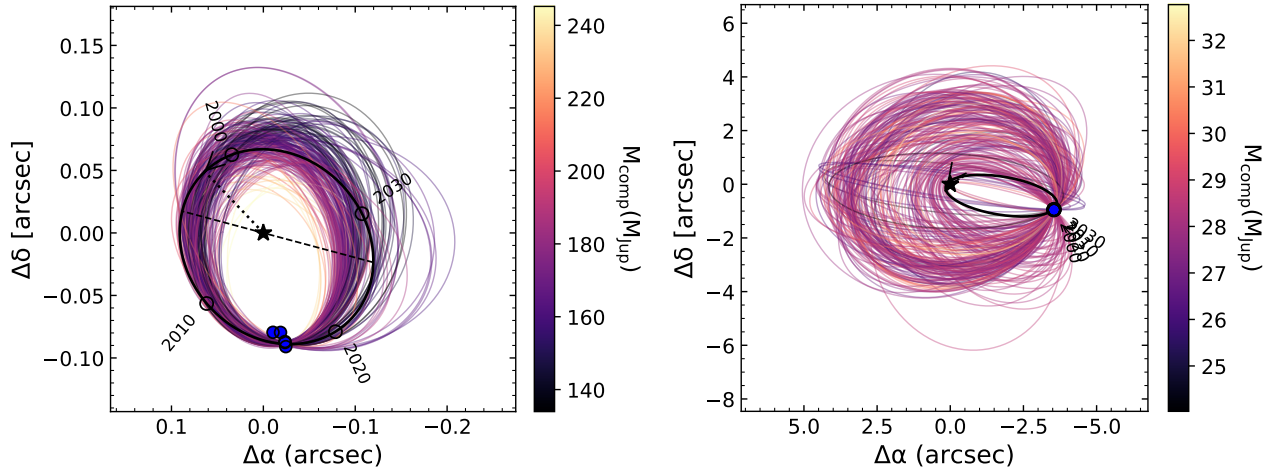


Figure 8. The relative astrometric orbit of HD 284149 B (*left*) and HD 284149 AB b (*right*). The thick black line represents the highest likelihood orbit; the thin colored lines represent 200 orbits drawn randomly from the posterior distribution. Dark purple corresponds to a low companion mass and light yellow corresponds to a high companion mass. The dotted black line shows the periastron passage and the arrow at the periastron passage shows the direction of the orbit. The dashed line indicates the line of nodes. Predicted past and future relative astrometric points are shown by black circles with their respective years, while the observed relative astrometric points from VLT/SPHERE data (Bonavita et al. 2017) are shown by the blue-filled data point, where the measurement error is smaller than the plotted symbol.

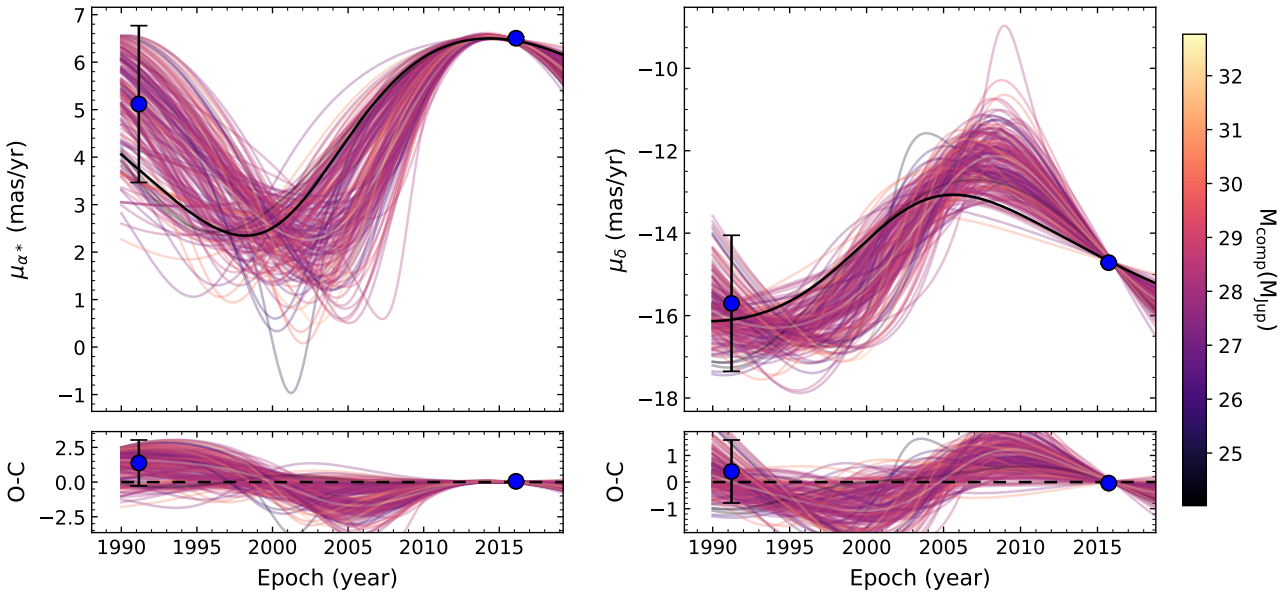


Figure 9. Acceleration induced by the companion on the host star as measured from absolute astrometry from Hipparcos and *Gaia*. The thick black line represents the highest likelihood orbit; the thin colored lines are 200 orbits drawn randomly from the posterior distribution. Darker purple represents a lower companion mass and light yellow represents a higher companion mass for HD 284149 AB b. The residuals of the proper motions are shown in the bottom panels.

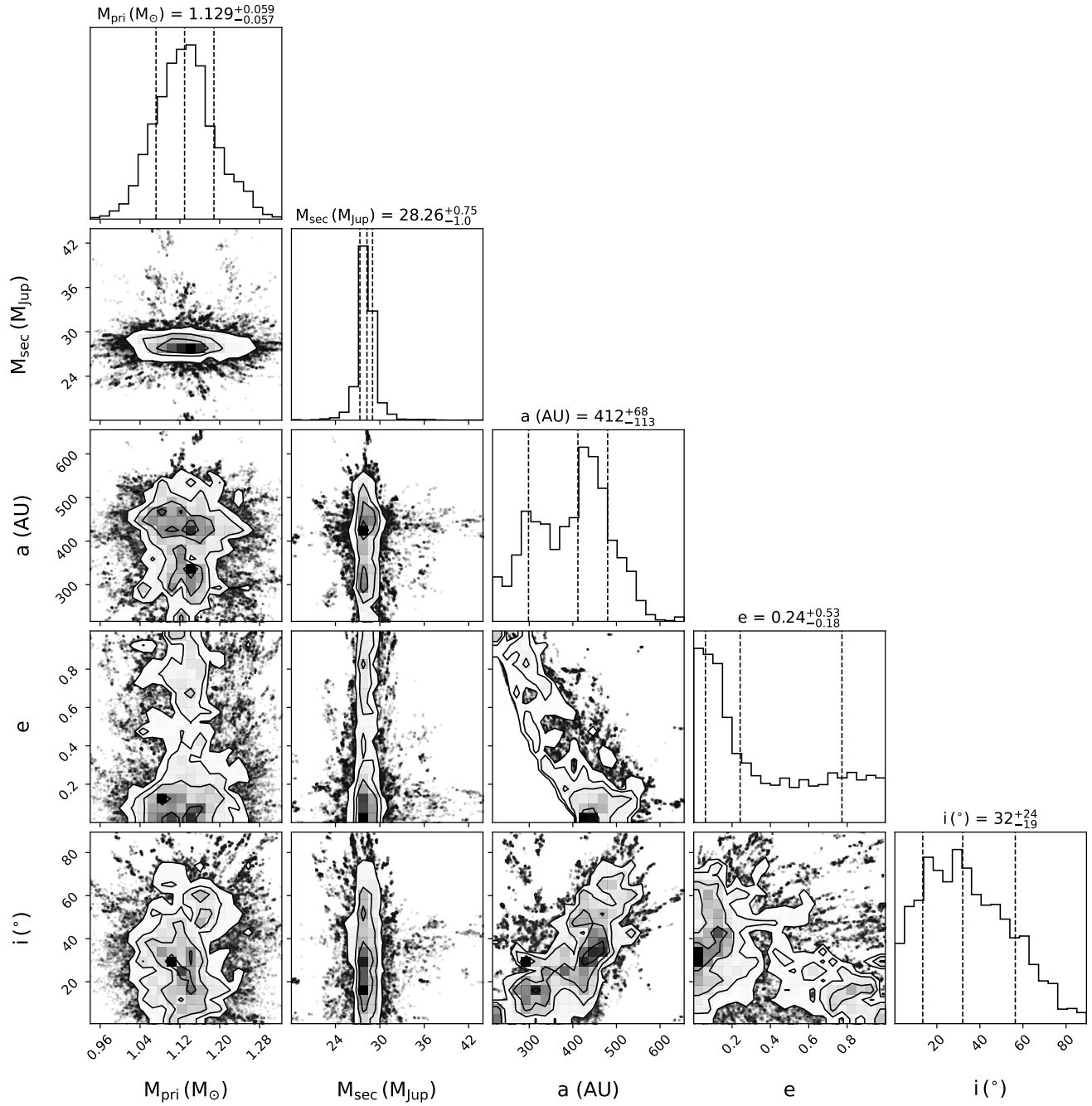


Figure 10. Corner plot showing the fitted orbital parameters for HD 284149 AB b using the orbit-fitting code `orvara` (Brandt et al. 2021).

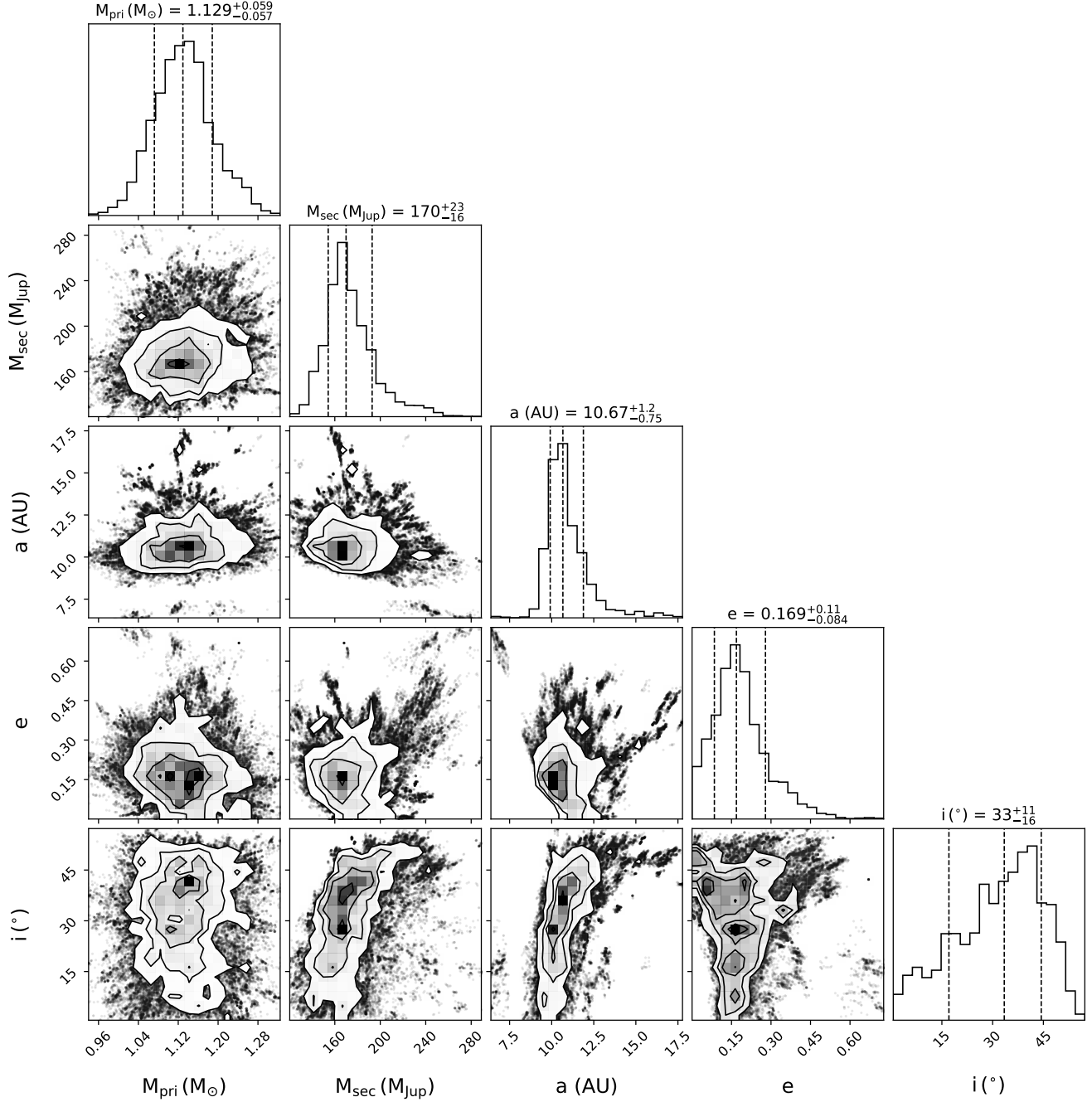


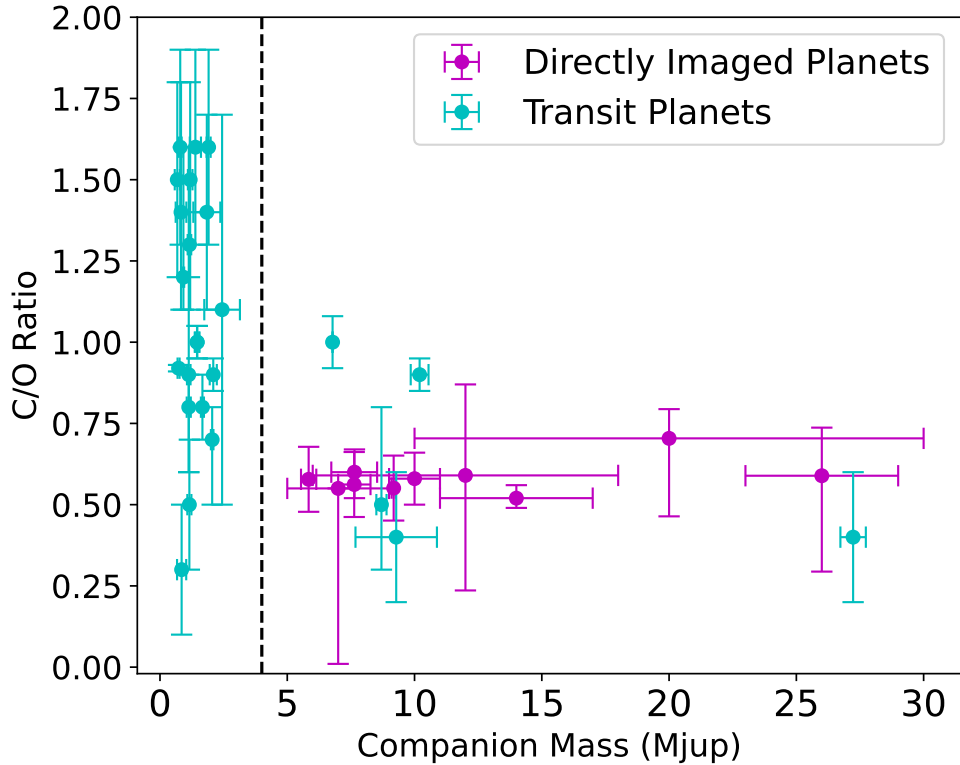
Figure 11. Corner plot showing the fitted orbital parameters for HD 284149 B using the orbit-fitting code `orvara` (Brandt et al. 2021).

ror ranges. We chose $4 M_{\text{Jup}}$ as the distinguishing mass, the central value between 3 and $5 M_{\text{Jup}}$. We then split the sample into two components, those with mass below $4 M_{\text{Jup}}$ and the other equal to or greater $4 M_{\text{Jup}}$. The two subsamples, with randomly sampled C/O ratios and corresponding randomly sampled masses were then put through the KS Test using the `scipy.stats.ks.2samp` Python package and the AD Test

using the `scipy.stats.anderson_ksamp` Python package. This generated 100,000 p values and significance values from each test. We show the resulting distributions in Figure 16. The results show that both p values and significance values are less than 1%, indicating that the two populations were distinct and statistically unlikely drawn from the same underlying population. We performed this same test for a cut off at $3 M_{\text{Jup}}$ and $5 M_{\text{Jup}}$,

Table 2. Log of two non-detected planets observed for the Imaging Spectroscopy Survey of Exoplanetary Atmospheres with Keck/OSIRIS.

Companion	Band	Spatial Sampling	Int. Time per	Total Number	Total Int. Time	Dates Taken
		(mas)	Frame (sec)	of Frames	(mins)	
51 Eri b	K	0.02	600	68	680	Nov 6-8, 2016 & Nov 3-4 2017
GJ 504 b	K	0.05	900	18	435	May 14, 2017 & May 26-27, 2019

**Figure 12.** Population of 25 transiting exoplanets (Changeat et al. 2022) in blue and 9 directly imaged planets in magenta. Shown here are their C/O ratios plotted against the companion masses in M_{Jup} . There appear to be two groupings of planets, one with masses below $4 M_{\text{Jup}}$ and one with masses greater than or equal to $4 M_{\text{Jup}}$, which is shown by the vertical dashed black line.

with results revealing that the p values and significance values are less than 1%. We also performed this test for just the transiting planets with a $4 M_{\text{Jup}}$ cut off, and found that the peak p values and significance values were less than 1%.

The values derived for C/O could be subject to additional systematics that are unaccounted for in the error bars provided in the literature. In particular, Changeat et al. (2022) show that different C/O ratios are derived in retrievals depending on which datasets are included in the fits. In order to try to account for these systematics, we performed the statistical similarity tests four

more times, inflating the transit/eclipse C/O ratio errors by 25%, 50%, 75%, and 100% respectively. We chose to inflate the transiting planet error bars but not the directly imaged planets because the former have much smaller uncertainties than the directly imaged planets, and are likely driving the visual distinction between the two populations of planets. For these four tests with inflated error bars, we found the same result with p values and significance values that were less than 1%, indicating the populations are statistically distinct.

The transit/eclipse and directly imaged planets overlap in mass, but not in separation, due to detection sen-

Table 3. Directly Imaged and Transit/Eclipse System and Atmospheric Parameters

Companion	Separation (au)	Age (Myr)	Companion Mass (M_{Jup})	Host Mass (M_{\odot})	C/O	References
Directly Imaged Planets						
κ And b	55±2	47±40	20±10	2.8±0.4	0.704 ^{+0.09} _{-0.24}	1, 2, 3, 4
VHS 1256 b	180±9	200±100	12±6	0.152±0.01	0.590 ^{+0.28} _{-0.24}	5, 6, 7
HD 284149 AB b	431±7	35±10	26 ± 3	1.13±0.06	0.589 ^{+0.148} _{-0.295}	8, 9
HR 8799 b	68±2	40±5	5.84 ± 0.3	1.47 ^{+0.12} _{-0.17}	0.578 ^{+0.004} _{-0.005}	10, 64, 11, 12, 13, 65, 66
HR 8799 c	42.81±1.16	40±5	7.63 ^{+0.64} _{-0.63}	1.47 ^{+0.12} _{-0.17}	0.562±0.004	10, 11, 12, 13, 65, 66
HR 8799 d	26.97±0.73	40±5	9.81±0.08	1.47 ^{+0.12} _{-0.17}	0.551 ^{+0.005} _{-0.004}	10, 11, 12, 13, 65, 66
HR 8799 e	17±0.5	40±5	7.64 ^{+0.89} _{-0.91}	1.47 ^{+0.12} _{-0.17}	0.60 ^{+0.07} _{-0.08}	10, 11, 12, 14, 65, 66
HIP 65426 b	92.3±0.2	14±3	7±2	1.96±0.04	0.55 ⁺⁰ _{-0.55}	16, 15
TYC 8998-760-1 b	162±0.28	16.7±1.4	14±3	1.00±0.02	0.52 ^{+0.04} _{-0.03}	17, 18
AB Pic b	273±2	13.3±1.1	10±1	0.84±0.11	0.58±0.08	21, 22, 23, 19
Transiting Planets						
CoRot-1 b	0.0261±0.0005	1600±500	1.13±0.07	1.22±0.03	0.9 ^{+0.7} _{-0.3}	24, 25, 26, 27
HAT-P-2 b	0.06814±0.00051	1440±470	8.7±0.2	1.33±0.03	0.5 ^{+0.3} _{-0.2}	28, 26, 27
HAT-P-7 b	0.03813±0.00036	2070±300	1.84±0.53	1.51±0.04	1.4 ^{+0.3} _{-0.3}	29, 26, 27
HAT-P-32 b	0.03397±0.00051	2700±800	0.68±0.1	1.132±0.05	1.5 ^{+0.3} _{-0.3}	30, 31, 27
HAT-P-41 b	0.04258±0.00047	2200±400	0.795±0.056	1.418±0.047	1.6 ^{+0.3} _{-0.3}	32, 26, 27
HAT-P-70 b	0.04739±0.00031	600±30	6.78±0	1.89±0.01	1 ^{+0.08} _{-0.08}	33, 27
HD 189733 b	0.03126±0.00036	6800±500	1.13±0.08	0.812±0.04	0.8 ^{+0.1} _{-0.2}	34, 35, 36, 27
HD 209458 b	0.04634±0.0007	3100±800	0.73±0.04	1.19±0.28	0.92 ^{+0.01} _{-0.01}	37, 26, 38, 27
KELT-1 b	0.02466±0.00016	n/a	27.23±0.5	1.3766±0.25	0.4 ^{+0.2} _{-0.2}	39, 40, 27
KELT-7 b	0.04415±0.0006	1300±200	1.39±0.22	1.45±0.05	1.6 ^{+0.3} _{-0.3}	41, 35, 40, 27
KELT-9 b	0.03462±0.001	n/a	2.44±0.7	2.431±0.3	1.1 ^{+0.6} _{-0.6}	42, 40, 27
Kepler-13A b	0.03641±0.00087	1120±100	9.28±1.6	1.67±0.08	0.4 ^{+0.2} _{-0.2}	43, 44, 45, 27
TrES-3 b	0.02282±0.0003	1000±500	1.91±0.08	0.820181±0.045	1.6 ^{+0.3} _{-0.3}	46, 26, 40, 27
WASP-4 b	0.0226±0.0007	7000±2900	1.186±0.09	0.97±0.150455	1.5 ^{+0.3} _{-0.4}	47, 48, 27
WASP-12 b	0.0232±0.00064	2000±700	1.465±0.079	1.17±0.183504	1 ^{+0.05} _{-0.05}	49, 50, 40, 27
WASP-18 b	0.02024±0.0003	1570±1000	10.2±0.35	1.294±0.06	0.9 ^{+0.05} _{-0.05}	51, 52, 27
WASP-19 b	0.01652±0.0005	6400±4000	1.154±0.08	0.965±0.091	0.5 ^{+0.2} _{-0.2}	53, 52, 27
WASP-33 b	0.0239±0.00063	n/a	2.093±0.139	1.653±0.349901	0.9 ^{+0.05} _{-0.05}	54, 50, 27
WASP-43 b	0.01528±0.00018	7000±7000	2.05±0.05	0.65±0.105	0.7 ^{+0.1} _{-0.2}	55, 26, 27
WASP-74 b	0.3443±0.00036	4200±1600	0.826±0.21	1.044±0.152063	1.4 ^{+0.4} _{-0.3}	56, 57, 27
WASP-76 b	0.033±0.0005	5300±6000	0.92±0.03	1.226±0.2333546	1.2 ^{+0.4} _{-0.1}	58, 40
WASP-77 A b	0.02335±0.00045	6200±4000	1.667±0.06	0.91±0.025	0.8 ^{+0.1} _{-0.1}	59, 52, 27
WASP-79 b	0.519±0.0008	1920±350	0.85±0.18	1.54±0.36	0.3 ^{+0.2} _{-0.2}	60, 40, 26, 27
WASP-103 b	0.01987±0.00021	4000±1000	1.455±0.09	1.22±0.039	1 ^{+0.05} _{-0.05}	61, 26, 27
WASP-121 b	0.02596±0.00063	1500±1000	1.157±0.07	1.368±0.084	1.3 ^{+0.1} _{-0.1}	62, 63, 27

References—(1) Carson et al. (2013), (2) Jones et al. (2016), (3) Hinkley et al. (2013), (4) Wilcomb et al. (2020), (5) Gauza et al. (2015), (6) Dupuy et al. (2023), (7) Hoch et al. (2022), (8) Bonavita et al. (2014), (9) Bonavita et al. (2017), (10) Marois et al. (2008), (11) Zuckerman et al. (2011), (12) Konopacky et al. (2013), (13) Ruffio et al. (2021), (14) Mollière et al. (2020), (15) Petrus et al. (2021), (16) Chauvin et al. (2017), (17) Bohn et al. (2020), (18) Zhang et al. (2021), (19) Palma-Bifani et al. (2022), (20) Booth et al. (2021), (21) Chauvin et al. (2005), (22) Bonnefoy et al. (2010), (23) Bonnefoy et al. (2014), (24) Barge et al. (2008), (25) Pont et al. (2010), (26) Bonomo et al. (2017), (27) Changeat et al. (2022), (28) Bakos et al. (2007), (29) Pál et al. (2008), (30) Hartman et al. (2011), (31) Wang et al. (2019), (32) Hartman et al. (2012), (33) Zhou et al. (2019), (34) Bouchy et al. (2005), (35) Stassun et al. (2017), (36) Addison et al. (2019), (37) Henry et al. (2000), (38) Rosenthal et al. (2021), (39) Siverd et al. (2012), (40) Stassun et al. (2019), (41) Bieryla et al. (2015), (42) Gaudi et al. (2017), (43) Borucki et al. (2011), (44) Esteves et al. (2015), (45) Morton et al. (2016), (46) O’Donovan et al. (2007), (47) Wilson et al. (2008), (48) Bouma et al. (2019), (49) Hebb et al. (2009), (50) Chakrabarty & Sengupta (2019), (51) Hellier et al. (2009), (52) Cortés-Zuleta et al. (2020), (53) Hebb et al. (2010), (54) Collier Cameron et al. (2010), (55) Hellier et al. (2011), (56) Hellier et al. (2015), (57) Mancini et al. (2019), (58) West et al. (2016), (59) Maxted et al. (2013), (60) Smalley et al. (2012), (61) Gillon et al. (2014), (62) Delrez et al. (2016), (63) Bourrier et al. (2020), (64) Bell et al. (2015), (65) Zurlo et al. (2022), (sss) Sepulveda & Bowler (2022)

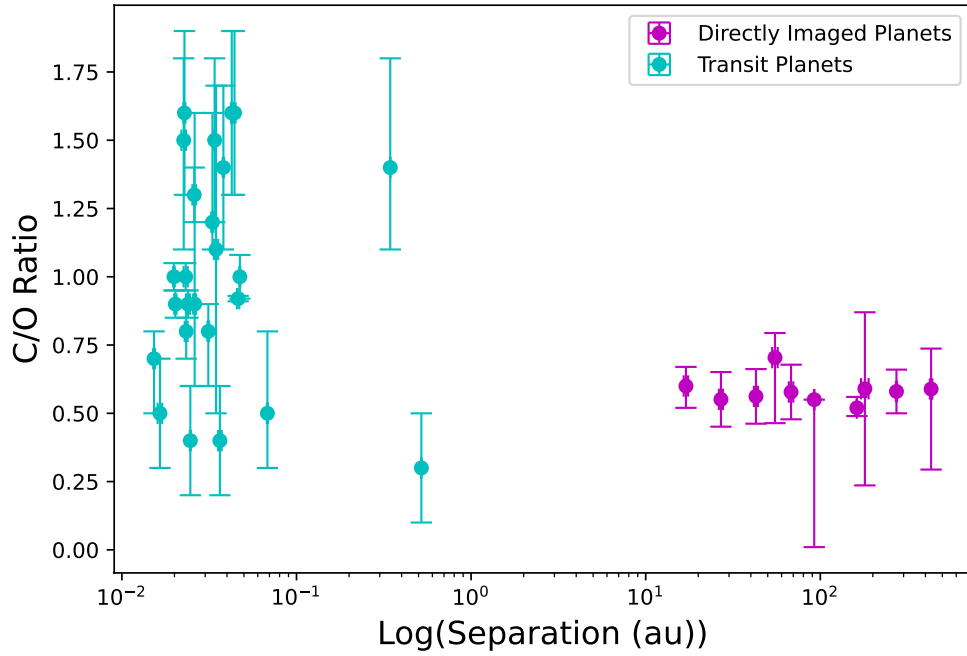


Figure 13. Population of 25 retrieval exoplanets in blue and 9 directly imaged planets in magenta. Here are their C/O ratios plotted against their projected separation in au from their host star/system. This plot illustrates highlights the sensitivity to different regions of separation space in each detection methodology for transiting and directly imaged planets. It also highlights how all directly imaged planets thus far have very consistent C/O ratios, which is not the case for the transiting planets.

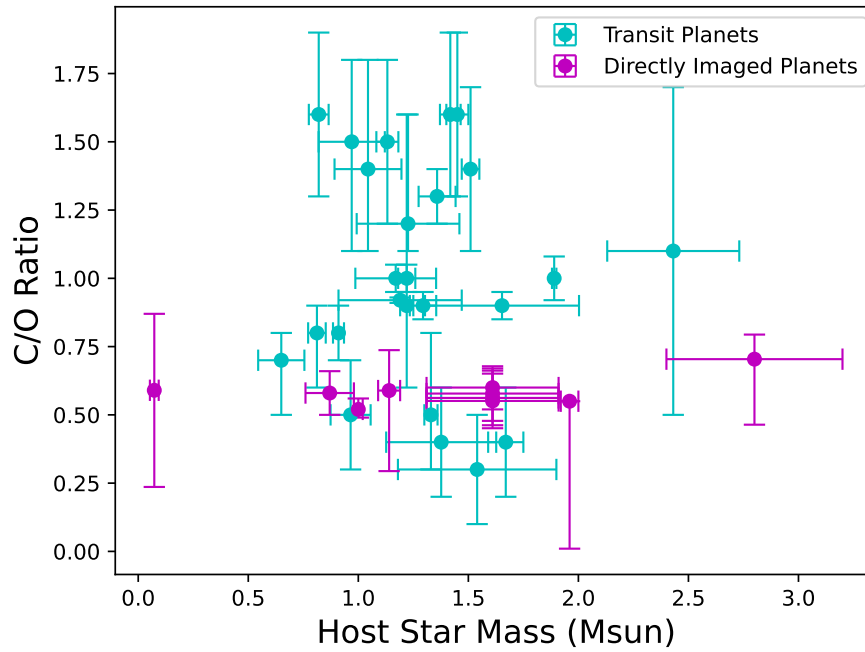


Figure 14. Population of 25 retrieval exoplanets in blue and 9 directly imaged planets in magenta. Here are their C/O ratios plotted against the host star masses in M_{\odot} . There seems to be no visible correlation between these parameters.

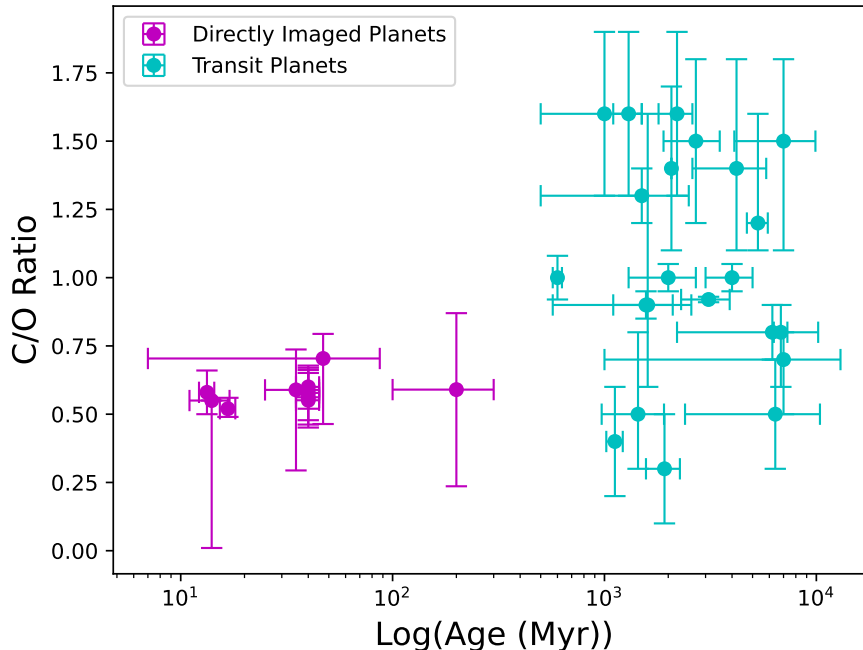


Figure 15. Population of 25 retrieval exoplanets in blue and 9 directly imaged planets in magenta. Here are their C/O ratios plotted against the system age in Myr. This illustrates the differences in the two populations, with the directly imaged planets being younger because they are more luminous and more easily detectable with direct imaging. Even with this distinction, the correlation most likely is not with age, but with either companion mass or with semimajor axis.

sitivities, making mass a more interesting parameter to explore. However, we do note that Figure 13 shows a visual difference in C/O ratio with separation, highlighting that all the directly imaged planet C/O ratios are very consistent with each other thus far. Even those this visual difference may be driven entirely by detection biases, we also ran these two tests for C/O ratio versus separation (au) and obtained a similar result with both p values and significance values less than 1%.

5. DISCUSSION

5.1. Implications for HD 284149 AB b

HD 284149 AB b is an interesting case for detailed atmospheric characterization because of its wide separation, youth, and brightness. Such objects that are easier to observe can provide insights into higher contrast systems for which it is difficult to obtain moderate resolution spectra. Our results of $T_{\text{eff}} = 2502 \text{ K}$, with a range of 2291–2624 K, $\log g = 4.52$, with a range of 4.38–4.91, and $[M/H] = 0.37$, with a range of 0.10–0.55 agree with the results from Bonavita et al. (2014, 2017) that posit HD 284149 AB b is likely a brown dwarf mass object, in a young system. We compared our results to Baraffe et al. (2015) evolutionary models assuming an age of 25 Myr and found a corresponding mass range of

27–38 M_{Jup} , which is consistent with $26 \pm 3 M_{\text{Jup}}$ from Bonavita et al. (2017).

Formation of objects in the same mass regime as gas giant planets and low mass brown dwarfs is of considerable interest because formation models have trouble producing these types of objects. Formation diagnostics such as C/O ratio can provide context as to where and potentially how these substellar objects have formed. HD 284149 AB b shares properties with imaged objects like AB Pic b (Chauvin et al. 2005) and ROXs 42Bb (Kraus et al. 2014), which place HD 284149 AB b between the planetary mass object regime and the lowest mass brown dwarfs imaged to date. HD 284149 AB b represents a challenge in our understanding of formation of low-mass companions at extremely wide separations. The low mass ratio of this system might point towards a planet-like formation scenario such as core/pebble accretion, but its estimated mass is quite high, which could suggest a star-like rapid formation process such as gravitational instability.

Measuring an approximately solar C/O ratio of HD 284149 AB b provides one possible diagnostic for understanding how this object formed. This result points to a very rapid formation process, potentially through either gravitational instability or common gravitational collapse similar to a binary star system. However, this

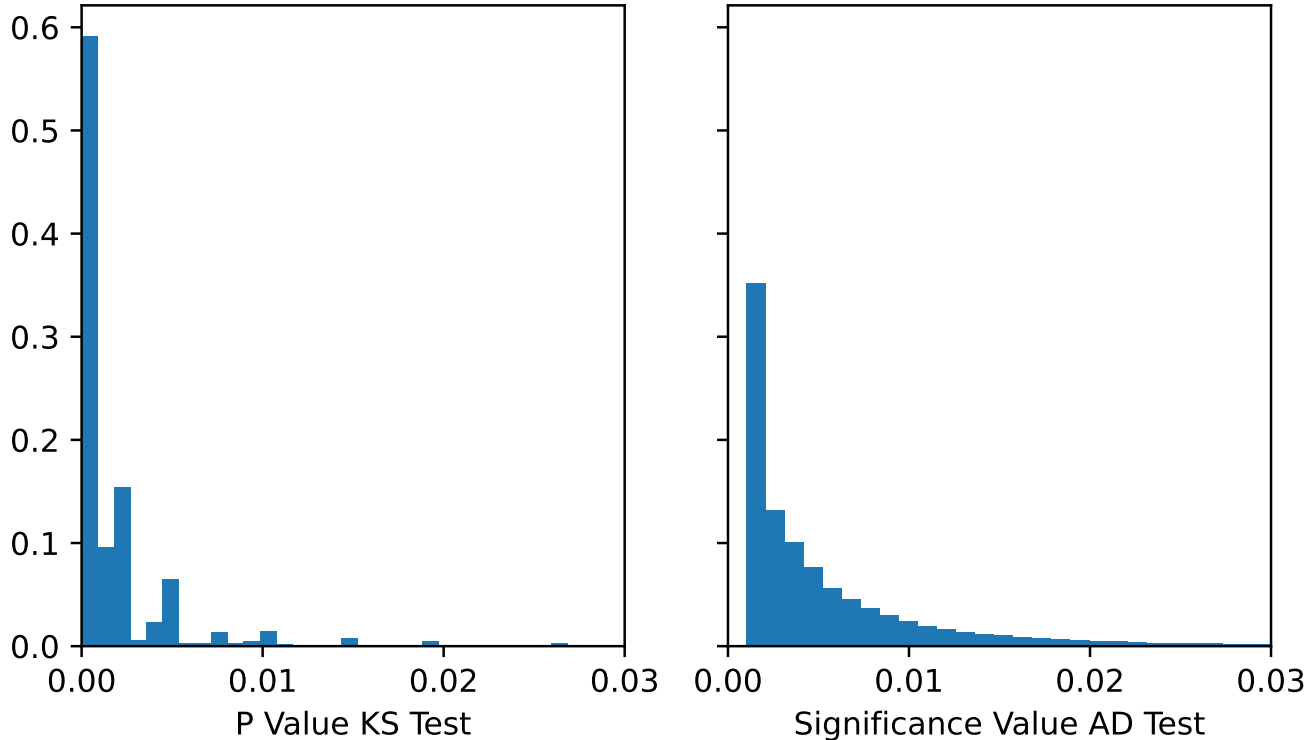


Figure 16. A histogram of p values from the KS Test and significance values from the AD Test. The results seem to show that both p values and significance values are less than 1% indicating that the two populations were distinct and not from the same underlying population.

diagnostic involves a comparison to the host star in order to draw definitive conclusions about formation. We do not have a C/O ratio of the host star because the data available were low resolution only. The slightly elevated metallicity could shed some light on formation, but host star metallicity is still required. Until atmospheric characterization is conducted on HD 284149 A, we can only conclude that the evidence points to roughly similar values for the host star and the companion if the star has similar abundances to Solar.

HD 284149 AB b now represents a ninth directly imaged substellar companion, in addition to the four HR 8799 planets (Konopacky et al. 2013; Barman et al. 2015; Mollière et al. 2020; Ruffio et al. 2021), κ And b (Wilcomb et al. 2020), VHS 1256 b (Hoch et al. 2022), HIP 65426 b (Petruş et al. 2021), TYC 8998-760-1 b (YSES-1 b Zhang et al. 2021), and AB Pic b (Palma-Bifani et al. 2022) with an approximately solar C/O ratio. The diagnostic did not produce the elevated C/O that would have been a strong argument in favor of core/pebble accretion. Although the scenario certainly cannot be ruled out given the uncertainties in the data and the range of possible C/O ratios

predicted by core/pebble accretion models (e.g., Madhusudhan 2019).

5.2. Implications for the C/O Ratio Trend

All of the directly imaged planets with C/O ratios have estimated masses of $>4 M_{Jup}$. Santos et al. (2017) postulated that there may be two distinct populations of exoplanets that split at $4 M_{Jup}$ when comparing stellar metallicity [Fe/H] to companion mass M_{Jup} . When we look at C/O ratio versus a range of other system parameters, the only one that showed a potential pattern or correlation and was not caused by detection bias, was companion mass. This could point towards two distinct populations of exoplanets based on companion mass, rather than detection method. Interestingly, the split is around $4 M_{Jup}$, the same as in Santos et al. (2017). Schlaufman (2018) also shows that objects with masses $\leq 4 M_{Jup}$ orbit metal-rich solar-type stars, a property that may indicate a core/pebble accretion formation pathway. The results of our KS test and AD test show that these populations are distinct populations and could possibly point to two different formation mechanisms. We note that in order to confirm this trend, we must obtain more C/O ratios for lower mass directly imaged planets. There are a few directly im-

aged planets with estimated masses below $4 M_{Jup}$, such as 51 Eri b, [Macintosh et al. \(2015\)](#), but they have not yet had their C/O ratios measured. Though we tried to obtain a spectrum 51 Eri b with OSIRIS, it remains beyond the reach of that instrument’s capabilities. Such measurements, which might be possible with the newer generation of instruments such as KPIC on Keck [DeLorme et al. \(2021\)](#), may reveal whether the trend with mass holds.

Additionally, there are some outliers in the samples probed in Figure 12. In particular there is a large spread in C/O in the planets under $4 M_{Jup}$, all of which are computed with transit spectroscopy. This spread could have a physical meaning, or it could mean better constraints on C/O ratios are needed. Indeed, the large spread in C/O ratio demonstrated in [Changeat et al. \(2022\)](#) based on the dataset used for retrieval highlights the potential for systematic errors using currently available transit spectroscopy. *JWST*, and future facilities such as *ARIEL* and Extremely Large Telescopes (ELTs) will obtain tighter constraints on atmospheric species that trace the C/O value and could narrow this spread.

5.3. Implications for the C/O ratio as a Formation Tracer

The C/O ratio as a formation tracer may require a deeper understanding of the evolution of the protoplanetary disk. There are other mechanisms that can impact the C/O ratio that should be studied before connecting composition to formation of transiting and directly imaged planets. Migration paired with core/pebble accretion has been postulated to explain the final location and atmospheric composition of planets, but including the chemical evolution of the protoplanetary disk could reveal that less migration is needed to explain the chemical properties of the atmospheres ([Mollière et al. 2022](#)). The population of Hot Jupiter’s studied by [Changeat et al. \(2022\)](#) almost certainly underwent significant migration, which could play an important role in the evolution of their C/O ratios. When considering pebble accretion, the drift, evaporation, and accretion of pebbles reproduces planetary C/O values, but it is uncertain whether it can reproduce the high atmospheric metallicities that have been seen in some directly imaged planets such as HR 8799 e ([Mollière et al. 2020](#)). Therefore, it is important to have an understanding of the chemical composition and evolution of the protoplanetary disk to understand the composition of the disk gas and solids that ultimately build the planets we detect. Measuring the C/O ratio of planets is still important to highlight trends and dichotomies in the population of exoplanets, but tracing a formation pathway with these measurements

require better constraints on elemental abundances and more detailed evolutionary models and/or observations of the disk composition ([van der Marel et al. 2021](#)).

6. CONCLUSIONS

The C/O ratio is thought to be a tracer of planet formation. In this work, we presented a statistical analysis of the published C/O ratios of directly imaged exoplanets and compared them with an existing characterized sample of transiting exoplanets.

Using moderate-resolution spectroscopy, we have greatly expanded our knowledge of directly imaged companions by measuring their atmospheric parameters and C/O ratios. Here, we found HD 284149 AB b to have $T_{\text{eff}} = 2502 \text{ K}$, with a range of 2291–2624 K, $\log g = 4.52$, with a range of 4.38–4.91, and $[M/H] = 0.37$, with a range of 0.10–0.55 which is in agreement with the results from [Bonavita et al. \(2014, 2017\)](#). We measure the C/O ratio to be $0.589^{+0.148}_{-0.295}$. Without the ratio for the host star, we cannot conduct a complete formation tracer analysis, but an approximately solar C/O ratio could point towards a rapid formation process such as gravitational instability or common collapse.

After obtaining the C/O ratio for HD 284149 AB b, we add this measurement to the growing list of measured C/O ratios for directly imaged companions and compare these ratios to C/O ratios measured by [Changeat et al. \(2022\)](#) for a sample of 25 “Hot Jupiters”. We analyze C/O ratios versus various system parameters as shown in Figures 12–15 and see a trend when looking at Companion Mass (M_{Jup}) versus C/O ratio, where there are two distinct groups of companions separated at $4 M_{Jup}$. We conduct a KS Test and AD Test to show that these groups of objects do not come from the same underlying population. This result could reveal that there are two distinct groups of companions that form through different methods.

Population studies of exoplanets and their formation pathways still remain difficult due to detection biases from each of the discovery methods. C/O ratio measurements for both transiting exoplanets and directly imaged exoplanets are also very difficult to measure using ground-based observatories. However, our imaging spectroscopy survey of exoplanetary atmospheres with Keck/OSIRIS has provided six out of the nine measured C/O ratios for directly imaged companions. To increase the number of C/O ratios measured, and improve the constraints on these measurements, space-based observatories such as *JWST* will provide increased wavelength coverage and higher signal-to-noise data for both transiting and directly imaged companions. The work presented here will pave the way for future studies based

on the next generation of space telescopes, high resolution spectrographs, and ELTs.

7. ACKNOWLEDGMENTS

The authors thank the anonymous referee for aiding in the publication of this work. The authors would like to thank Randy Campbell, Heather Hershley, and Tony Connors for their support in obtaining these observations. K.K.W.H., Q.M.K, and T.S.B acknowledge support by the National Aeronautics and Space Administration under Grants/Contracts/Agreements No.NNX17AB63G and 80NSSC21K0573 issued through the Astrophysics Division of the Science Mission Directorate. T.S.B. acknowledges support by the National Science Foundation under Grant No. 1614492. Any opinions, findings, conclusions, and/or recommendations expressed in this paper are those of the author(s) and do not reflect the views of the National Aeronautics and Space Administration. The data presented herein

were obtained at the W. M. Keck Observatory, which is operated as a scientific partnership among the California Institute of Technology, the University of California, and the National Aeronautics and Space Administration. The W. M. Keck Observatory was made possible by the financial support of the W. M. Keck Foundation. The authors wish to acknowledge the significant cultural role that the summit of Maunakea has always had within the indigenous Hawaiian community. The author(s) are extremely fortunate to conduct observations from this mountain. Portions of this work were conducted at the University of California, San Diego, which was built on the unceded territory of the Kumeyaay Nation, whose people continue to maintain their political sovereignty and cultural traditions as vital members of the San Diego community.

Facilities: Keck/OSIRIS

Software: *emcee* (Foreman-Mackey et al. 2013), *SMART* (Hsu et al. 2021a,b), *orvara* (Brandt et al. 2021)

REFERENCES

- Addison, B., Wright, D. J., Wittenmyer, R. A., et al. 2019, *PASP*, 131, 115003, doi: [10.1088/1538-3873/ab03aa](https://doi.org/10.1088/1538-3873/ab03aa)
- Ali-Dib, M., Mousis, O., Pekmezci, G. S., et al. 2014, *A&A*, 561, A60, doi: [10.1051/0004-6361/201321780](https://doi.org/10.1051/0004-6361/201321780)
- Bakos, G. Á., Kovács, G., Torres, G., et al. 2007, *ApJ*, 670, 826, doi: [10.1086/521866](https://doi.org/10.1086/521866)
- Baraffe, I., Homeier, D., Allard, F., & Chabrier, G. 2015, *A&A*, 577, A42, doi: [10.1051/0004-6361/201425481](https://doi.org/10.1051/0004-6361/201425481)
- Barge, P., Baglin, A., Auvergne, M., et al. 2008, *A&A*, 482, L17, doi: [10.1051/0004-6361:200809353](https://doi.org/10.1051/0004-6361:200809353)
- Barman, T. S., Konopacky, Q. M., Macintosh, B., & Marois, C. 2015, *ApJ*, 804, 61, doi: [10.1088/0004-637X/804/1/61](https://doi.org/10.1088/0004-637X/804/1/61)
- Barman, T. S., Macintosh, B., Konopacky, Q. M., & Marois, C. 2011, *ApJ*, 733, 65, doi: [10.1088/0004-637X/733/1/65](https://doi.org/10.1088/0004-637X/733/1/65)
- Bell, C. P. M., Mamajek, E. E., & Naylor, T. 2015, *MNRAS*, 454, 593, doi: [10.1093/mnras/stv1981](https://doi.org/10.1093/mnras/stv1981)
- Bergemann, M., Kudritzki, R.-P., Plez, B., et al. 2012, *ApJ*, 751, 156, doi: [10.1088/0004-637X/751/2/156](https://doi.org/10.1088/0004-637X/751/2/156)
- Bieryla, A., Collins, K., Beatty, T. G., et al. 2015, *AJ*, 150, 12, doi: [10.1088/0004-6256/150/1/12](https://doi.org/10.1088/0004-6256/150/1/12)
- Biller, B. A., Liu, M. C., Wahhaj, Z., et al. 2013, *ApJ*, 777, 160, doi: [10.1088/0004-637X/777/2/160](https://doi.org/10.1088/0004-637X/777/2/160)
- Blake, C. H., Charbonneau, D., & White, R. J. 2010, *ApJ*, 723, 684, doi: [10.1088/0004-637X/723/1/684](https://doi.org/10.1088/0004-637X/723/1/684)
- Bodenheimer, P., & Pollack, J. B. 1986, *Icarus*, 67, 391, doi: [10.1016/0019-1035\(86\)90122-3](https://doi.org/10.1016/0019-1035(86)90122-3)
- Bohn, A. J., Kenworthy, M. A., Ginski, C., et al. 2020, *MNRAS*, 492, 431, doi: [10.1093/mnras/stz3462](https://doi.org/10.1093/mnras/stz3462)
- Bonavita, M., Daemgen, S., Desidera, S., et al. 2014, *ApJL*, 791, L40, doi: [10.1088/2041-8205/791/2/L40](https://doi.org/10.1088/2041-8205/791/2/L40)
- Bonavita, M., D’Orazi, V., Mesa, D., et al. 2017, *A&A*, 608, A106, doi: [10.1051/0004-6361/201731003](https://doi.org/10.1051/0004-6361/201731003)
- Bonnefoy, M., Chauvin, G., Lagrange, A. M., et al. 2014, *A&A*, 562, A127, doi: [10.1051/0004-6361/201118270](https://doi.org/10.1051/0004-6361/201118270)
- Bonnefoy, M., Chauvin, G., Rojo, P., et al. 2010, *A&A*, 512, A52, doi: [10.1051/0004-6361/200912688](https://doi.org/10.1051/0004-6361/200912688)
- Bonomo, A. S., Desidera, S., Benatti, S., et al. 2017, *A&A*, 602, A107, doi: [10.1051/0004-6361/201629882](https://doi.org/10.1051/0004-6361/201629882)
- Booth, A. S., van der Marel, N., Leemker, M., van Dishoeck, E. F., & Ohashi, S. 2021, *A&A*, 651, L6, doi: [10.1051/0004-6361/202141057](https://doi.org/10.1051/0004-6361/202141057)
- Booth, R. A., Clarke, C. J., Madhusudhan, N., & Ilee, J. D. 2017, *MNRAS*, 469, 3994, doi: [10.1093/mnras/stx1103](https://doi.org/10.1093/mnras/stx1103)
- Borucki, W. J., Koch, D. G., Basri, G., et al. 2011, *ApJ*, 736, 19, doi: [10.1088/0004-637X/736/1/19](https://doi.org/10.1088/0004-637X/736/1/19)
- Boucher, A., Lafrenière, D., Pelletier, S., et al. 2023, *MNRAS*, 522, 5062, doi: [10.1093/mnras/stad1247](https://doi.org/10.1093/mnras/stad1247)
- Bouchy, F., Udry, S., Mayor, M., et al. 2005, *A&A*, 444, L15, doi: [10.1051/0004-6361:200500201](https://doi.org/10.1051/0004-6361:200500201)
- Bouma, L. G., Winn, J. N., Baxter, C., et al. 2019, *AJ*, 157, 217, doi: [10.3847/1538-3881/ab189f](https://doi.org/10.3847/1538-3881/ab189f)

- Bourrier, V., Ehrenreich, D., Lendl, M., et al. 2020, *A&A*, 635, A205, doi: [10.1051/0004-6361/201936640](https://doi.org/10.1051/0004-6361/201936640)
- Brandt, T. D. 2021, *ApJS*, 254, 42, doi: [10.3847/1538-4365/abf93c](https://doi.org/10.3847/1538-4365/abf93c)
- Brandt, T. D., Dupuy, T. J., Li, Y., et al. 2021, *AJ*, 162, 186, doi: [10.3847/1538-3881/ac042e](https://doi.org/10.3847/1538-3881/ac042e)
- Brown-Sevilla, S. B., Maire, A. L., Mollière, P., et al. 2023, *A&A*, 673, A98, doi: [10.1051/0004-6361/202244826](https://doi.org/10.1051/0004-6361/202244826)
- Burgasser, A. J., Lopez, M. A., Mamajek, E. E., et al. 2016, *ApJ*, 820, 32, doi: [10.3847/0004-637X/820/1/32](https://doi.org/10.3847/0004-637X/820/1/32)
- Cameron, A. G. W. 1978, *Moon and Planets*, 18, 5, doi: [10.1007/BF00896696](https://doi.org/10.1007/BF00896696)
- Carson, J., Thalmann, C., Janson, M., et al. 2013, *ApJL*, 763, L32, doi: [10.1088/2041-8205/763/2/L32](https://doi.org/10.1088/2041-8205/763/2/L32)
- Chakrabarty, A., & Sengupta, S. 2019, *AJ*, 158, 39, doi: [10.3847/1538-3881/ab24dd](https://doi.org/10.3847/1538-3881/ab24dd)
- Changeat, Q., Al-Refaie, A., Mugnai, L. V., et al. 2020, *AJ*, 160, 80, doi: [10.3847/1538-3881/ab9a53](https://doi.org/10.3847/1538-3881/ab9a53)
- Changeat, Q., Edwards, B., Al-Refaie, A. F., et al. 2022, *ApJS*, 260, 3, doi: [10.3847/1538-4365/ac5cc2](https://doi.org/10.3847/1538-4365/ac5cc2)
- Charnay, B., Bézard, B., Baudino, J. L., et al. 2018, *ApJ*, 854, 172, doi: [10.3847/1538-4357/aaac7d](https://doi.org/10.3847/1538-4357/aaac7d)
- Chatterjee, S., Ford, E. B., Matsumura, S., & Rasio, F. A. 2008, *ApJ*, 686, 580, doi: [10.1086/590227](https://doi.org/10.1086/590227)
- Chauvin, G., Lagrange, A. M., Zuckerman, B., et al. 2005, *A&A*, 438, L29, doi: [10.1051/0004-6361:200500111](https://doi.org/10.1051/0004-6361:200500111)
- Chauvin, G., Desidera, S., Lagrange, A. M., et al. 2017, *A&A*, 605, L9, doi: [10.1051/0004-6361/201731152](https://doi.org/10.1051/0004-6361/201731152)
- Collier Cameron, A., Guenther, E., Smalley, B., et al. 2010, *MNRAS*, 407, 507, doi: [10.1111/j.1365-2966.2010.16922.x](https://doi.org/10.1111/j.1365-2966.2010.16922.x)
- Cortés-Zuleta, P., Rojo, P., Wang, S., et al. 2020, *A&A*, 636, A98, doi: [10.1051/0004-6361/201936279](https://doi.org/10.1051/0004-6361/201936279)
- Cridland, A. J., van Dishoeck, E. F., Alessi, M., & Pudritz, R. E. 2019, *A&A*, 632, A63, doi: [10.1051/0004-6361/201936105](https://doi.org/10.1051/0004-6361/201936105)
- Currie, T., Burrows, A., Itoh, Y., et al. 2011, *ApJ*, 729, 128, doi: [10.1088/0004-637X/729/2/128](https://doi.org/10.1088/0004-637X/729/2/128)
- Daemgen, S., Bonavita, M., Jayawardhana, R., Lafrenière, D., & Janson, M. 2015, *ApJ*, 799, 155, doi: [10.1088/0004-637X/799/2/155](https://doi.org/10.1088/0004-637X/799/2/155)
- Delorme, J.-R., Jovanovic, N., Echeverri, D., et al. 2021, *Journal of Astronomical Telescopes, Instruments, and Systems*, 7, 035006, doi: [10.1117/1.JATIS.7.3.035006](https://doi.org/10.1117/1.JATIS.7.3.035006)
- Delrez, L., Santerne, A., Almenara, J. M., et al. 2016, *MNRAS*, 458, 4025, doi: [10.1093/mnras/stw522](https://doi.org/10.1093/mnras/stw522)
- Do Ó, C. R., O’Neil, K. K., Konopacky, Q. M., et al. 2023, *arXiv e-prints*, arXiv:2306.04080, doi: [10.48550/arXiv.2306.04080](https://doi.org/10.48550/arXiv.2306.04080)
- D’Orazi, V., Biazzo, K., & Randich, S. 2011, *A&A*, 526, A103, doi: [10.1051/0004-6361/201015616](https://doi.org/10.1051/0004-6361/201015616)
- Dupuy, T. J., Liu, M. C., Evans, E. L., et al. 2023, *MNRAS*, 519, 1688, doi: [10.1093/mnras/stac3557](https://doi.org/10.1093/mnras/stac3557)
- Eistrup, C., Walsh, C., & van Dishoeck, E. F. 2018, *A&A*, 613, A14, doi: [10.1051/0004-6361/201731302](https://doi.org/10.1051/0004-6361/201731302)
- Esteves, L. J., De Mooij, E. J. W., & Jayawardhana, R. 2015, *ApJ*, 804, 150, doi: [10.1088/0004-637X/804/2/150](https://doi.org/10.1088/0004-637X/804/2/150)
- Ferrer-Chávez, R., Wang, J. J., & Blunt, S. 2021, *AJ*, 161, 241, doi: [10.3847/1538-3881/abf0a8](https://doi.org/10.3847/1538-3881/abf0a8)
- Finnerty, L., Schofield, T., Sappéy, B., et al. 2023, *arXiv e-prints*, arXiv:2305.19389, doi: [10.48550/arXiv.2305.19389](https://doi.org/10.48550/arXiv.2305.19389)
- Foreman-Mackey, D., Conley, A., Meierjürgen Farr, W., et al. 2013, *emcee: The MCMC Hammer*. <http://ascl.net/1303.002>
- Fortney, J. J., Shabram, M., Showman, A. P., et al. 2010, *ApJ*, 709, 1396, doi: [10.1088/0004-637X/709/2/1396](https://doi.org/10.1088/0004-637X/709/2/1396)
- Gaia Collaboration, Brown, A. G. A., Vallenari, A., et al. 2021, *A&A*, 649, A1, doi: [10.1051/0004-6361/202039657](https://doi.org/10.1051/0004-6361/202039657)
- Galicher, R., Marois, C., Macintosh, B., Barman, T., & Konopacky, Q. 2011, *ApJL*, 739, L41, doi: [10.1088/2041-8205/739/2/L41](https://doi.org/10.1088/2041-8205/739/2/L41)
- Galicher, R., Marois, C., Macintosh, B., et al. 2016, *A&A*, 594, A63, doi: [10.1051/0004-6361/201527828](https://doi.org/10.1051/0004-6361/201527828)
- Gaudi, B. S., Stassun, K. G., Collins, K. A., et al. 2017, *Nature*, 546, 514, doi: [10.1038/nature22392](https://doi.org/10.1038/nature22392)
- Gauza, B., Béjar, V. J. S., Pérez-Garrido, A., et al. 2015, *ApJ*, 804, 96, doi: [10.1088/0004-637X/804/2/96](https://doi.org/10.1088/0004-637X/804/2/96)
- Gillon, M., Anderson, D. R., Collier-Cameron, A., et al. 2014, *A&A*, 562, L3, doi: [10.1051/0004-6361/201323014](https://doi.org/10.1051/0004-6361/201323014)
- Goodman, J., & Weare, J. 2010, *Communications in Applied Mathematics and Computational Science*, 5, 65, doi: [10.2140/camcos.2010.5.65](https://doi.org/10.2140/camcos.2010.5.65)
- Gravity Collaboration, Abuter, R., Accardo, M., et al. 2017, *A&A*, 602, A94, doi: [10.1051/0004-6361/201730838](https://doi.org/10.1051/0004-6361/201730838)
- GRAVITY Collaboration, Nowak, M., Lacour, S., et al. 2020, *A&A*, 633, A110, doi: [10.1051/0004-6361/201936898](https://doi.org/10.1051/0004-6361/201936898)
- Hartman, J. D., Bakos, G. Á., Torres, G., et al. 2011, *ApJ*, 742, 59, doi: [10.1088/0004-637X/742/1/59](https://doi.org/10.1088/0004-637X/742/1/59)
- Hartman, J. D., Bakos, G. Á., Béky, B., et al. 2012, *AJ*, 144, 139, doi: [10.1088/0004-6256/144/5/139](https://doi.org/10.1088/0004-6256/144/5/139)
- Hebb, L., Collier-Cameron, A., Loeillet, B., et al. 2009, *ApJ*, 693, 1920, doi: [10.1088/0004-637X/693/2/1920](https://doi.org/10.1088/0004-637X/693/2/1920)
- Hebb, L., Collier-Cameron, A., Triaud, A. H. M. J., et al. 2010, *ApJ*, 708, 224, doi: [10.1088/0004-637X/708/1/224](https://doi.org/10.1088/0004-637X/708/1/224)
- Helled, R., & Schubert, G. 2009, *ApJ*, 697, 1256, doi: [10.1088/0004-637X/697/2/1256](https://doi.org/10.1088/0004-637X/697/2/1256)
- Hellier, C., Anderson, D. R., Collier Cameron, A., et al. 2009, *Nature*, 460, 1098, doi: [10.1038/nature08245](https://doi.org/10.1038/nature08245)
- . 2011, *A&A*, 535, L7, doi: [10.1051/0004-6361/201117081](https://doi.org/10.1051/0004-6361/201117081)

- . 2015, *AJ*, 150, 18, doi: [10.1088/0004-6256/150/1/18](https://doi.org/10.1088/0004-6256/150/1/18)
- Henry, G. W., Marcy, G. W., Butler, R. P., & Vogt, S. S. 2000, *ApJL*, 529, L41, doi: [10.1086/312458](https://doi.org/10.1086/312458)
- Hinkley, S., Pueyo, L., Faherty, J. K., et al. 2013, *ApJ*, 779, 153, doi: [10.1088/0004-637X/779/2/153](https://doi.org/10.1088/0004-637X/779/2/153)
- Hoch, K. K. W., Konopacky, Q. M., Barman, T. S., et al. 2022, arXiv e-prints, arXiv:2207.03819, <https://arxiv.org/abs/2207.03819>
- Hsu, C.-C., Theissen, C., Burgasser, A., & Birky, J. 2021a, SMART: The Spectral Modeling Analysis and RV Tool, v1.0.0, Zenodo, Zenodo, doi: [10.5281/zenodo.4765258](https://doi.org/10.5281/zenodo.4765258)
- Hsu, C.-C., Burgasser, A. J., Theissen, C. A., et al. 2021b, *ApJS*, 257, 45, doi: [10.3847/1538-4365/ac1c7d](https://doi.org/10.3847/1538-4365/ac1c7d)
- Husser, T. O., Wende-von Berg, S., Dreizler, S., et al. 2013, *A&A*, 553, A6, doi: [10.1051/0004-6361/201219058](https://doi.org/10.1051/0004-6361/201219058)
- Ikoma, M., Nakazawa, K., & Emori, H. 2000, *ApJ*, 537, 1013, doi: [10.1086/309050](https://doi.org/10.1086/309050)
- Ingraham, P., Marley, M. S., Saumon, D., et al. 2014, *ApJL*, 794, L15, doi: [10.1088/2041-8205/794/1/L15](https://doi.org/10.1088/2041-8205/794/1/L15)
- Johansen, A., & Lambrechts, M. 2017, *Annual Review of Earth and Planetary Sciences*, 45, 359, doi: [10.1146/annurev-earth-063016-020226](https://doi.org/10.1146/annurev-earth-063016-020226)
- Jones, J., White, R. J., Quinn, S., et al. 2016, *ApJL*, 822, L3, doi: [10.3847/2041-8205/822/1/L3](https://doi.org/10.3847/2041-8205/822/1/L3)
- Konopacky, Q. M., Barman, T. S., Macintosh, B. A., & Marois, C. 2013, *Science*, 339, 1398, doi: [10.1126/science.1232003](https://doi.org/10.1126/science.1232003)
- Kosmo O'Neil, K., Martinez, G. D., Hees, A., et al. 2019, *AJ*, 158, 4, doi: [10.3847/1538-3881/ab1d66](https://doi.org/10.3847/1538-3881/ab1d66)
- Krabbe, A., Gasaway, T., Song, I., et al. 2004, in *Society of Photo-Optical Instrumentation Engineers (SPIE) Conference Series*, Vol. 5492, Ground-based Instrumentation for Astronomy, ed. A. F. M. Moorwood & M. Iye, 1403–1410, doi: [10.1117/12.552592](https://doi.org/10.1117/12.552592)
- Kraus, A. L., Herczeg, G. J., Rizzuto, A. C., et al. 2017, *ApJ*, 838, 150, doi: [10.3847/1538-4357/aa62a0](https://doi.org/10.3847/1538-4357/aa62a0)
- Kraus, A. L., Ireland, M. J., Cieza, L. A., et al. 2014, *ApJ*, 781, 20, doi: [10.1088/0004-637X/781/1/20](https://doi.org/10.1088/0004-637X/781/1/20)
- Kuiper, G. P. 1951, *Proceedings of the National Academy of Science*, 37, 1, doi: [10.1073/pnas.37.1.1](https://doi.org/10.1073/pnas.37.1.1)
- Kuzuhara, M., Tamura, M., Kudo, T., et al. 2013, *ApJ*, 774, 11, doi: [10.1088/0004-637X/774/1/11](https://doi.org/10.1088/0004-637X/774/1/11)
- Larkin, J., Barczys, M., Krabbe, A., et al. 2006, in *Society of Photo-Optical Instrumentation Engineers (SPIE) Conference Series*, Vol. 6269, Society of Photo-Optical Instrumentation Engineers (SPIE) Conference Series, ed. I. S. McLean & M. Iye, 62691A, doi: [10.1117/12.672061](https://doi.org/10.1117/12.672061)
- Lavie, B., Mendonça, J. M., Mordasini, C., et al. 2017, *AJ*, 154, 91, doi: [10.3847/1538-3881/aa7ed8](https://doi.org/10.3847/1538-3881/aa7ed8)
- Lee, J.-M., Heng, K., & Irwin, P. G. J. 2013, *ApJ*, 778, 97, doi: [10.1088/0004-637X/778/2/97](https://doi.org/10.1088/0004-637X/778/2/97)
- Li, C., Ingersoll, A., Bolton, S., et al. 2020, *Nature Astronomy*, 4, 609, doi: [10.1038/s41550-020-1009-3](https://doi.org/10.1038/s41550-020-1009-3)
- Line, M. R., Knutson, H., Wolf, A. S., & Yung, Y. L. 2014, *ApJ*, 783, 70, doi: [10.1088/0004-637X/783/2/70](https://doi.org/10.1088/0004-637X/783/2/70)
- Line, M. R., Brogi, M., Bean, J. L., et al. 2021, *Nature*, 598, 580, doi: [10.1038/s41586-021-03912-6](https://doi.org/10.1038/s41586-021-03912-6)
- Lockhart, K. E., Do, T., Larkin, J. E., et al. 2019, *AJ*, 157, 75, doi: [10.3847/1538-3881/aaf64e](https://doi.org/10.3847/1538-3881/aaf64e)
- Luhman, K. L., Mamajek, E. E., Shukla, S. J., & Loutrel, N. P. 2017, *AJ*, 153, 46, doi: [10.3847/1538-3881/153/1/46](https://doi.org/10.3847/1538-3881/153/1/46)
- Macintosh, B., Graham, J. R., Barman, T., et al. 2015, *Science*, 350, 64, doi: [10.1126/science.aac5891](https://doi.org/10.1126/science.aac5891)
- Madhusudhan, N. 2012a, *ApJ*, 758, 36, doi: [10.1088/0004-637X/758/1/36](https://doi.org/10.1088/0004-637X/758/1/36)
- . 2012b, *ApJ*, 758, 36, doi: [10.1088/0004-637X/758/1/36](https://doi.org/10.1088/0004-637X/758/1/36)
- . 2019, *ARA&A*, 57, 617, doi: [10.1146/annurev-astro-081817-051846](https://doi.org/10.1146/annurev-astro-081817-051846)
- Madhusudhan, N., Amin, M. A., & Kennedy, G. M. 2014, *ApJL*, 794, L12, doi: [10.1088/2041-8205/794/1/L12](https://doi.org/10.1088/2041-8205/794/1/L12)
- Madhusudhan, N., Bitsch, B., Johansen, A., & Eriksson, L. 2017, *MNRAS*, 469, 4102, doi: [10.1093/mnras/stx1139](https://doi.org/10.1093/mnras/stx1139)
- Madhusudhan, N., Mousis, O., Johnson, T. V., & Lunine, J. I. 2011a, *ApJ*, 743, 191, doi: [10.1088/0004-637X/743/2/191](https://doi.org/10.1088/0004-637X/743/2/191)
- Madhusudhan, N., Harrington, J., Stevenson, K. B., et al. 2011b, *Nature*, 469, 64, doi: [10.1038/nature09602](https://doi.org/10.1038/nature09602)
- . 2011c, *Nature*, 469, 64, doi: [10.1038/nature09602](https://doi.org/10.1038/nature09602)
- Mancini, L., Southworth, J., Mollière, P., et al. 2019, *MNRAS*, 485, 5168, doi: [10.1093/mnras/stz661](https://doi.org/10.1093/mnras/stz661)
- Mansfield, M., Line, M. R., Bean, J. L., et al. 2021, *Nature Astronomy*, 5, 1224, doi: [10.1038/s41550-021-01455-4](https://doi.org/10.1038/s41550-021-01455-4)
- Marois, C., Macintosh, B., Barman, T., et al. 2008, *Science*, 322, 1348, doi: [10.1126/science.1166585](https://doi.org/10.1126/science.1166585)
- Maxted, P. F. L., Anderson, D. R., Collier Cameron, A., et al. 2013, *PASP*, 125, 48, doi: [10.1086/669231](https://doi.org/10.1086/669231)
- Mizuno, H., Nakazawa, K., & Hayashi, C. 1980, *Earth and Planetary Science Letters*, 50, 202, doi: [10.1016/0012-821X\(80\)90131-4](https://doi.org/10.1016/0012-821X(80)90131-4)
- Mollière, P., Wardenier, J. P., van Boekel, R., et al. 2019, *A&A*, 627, A67, doi: [10.1051/0004-6361/201935470](https://doi.org/10.1051/0004-6361/201935470)
- Mollière, P., Stolker, T., Lacour, S., et al. 2020, *A&A*, 640, A131, doi: [10.1051/0004-6361/202038325](https://doi.org/10.1051/0004-6361/202038325)
- Mollière, P., Molyarova, T., Bitsch, B., et al. 2022, *ApJ*, 934, 74, doi: [10.3847/1538-4357/ac6a56](https://doi.org/10.3847/1538-4357/ac6a56)
- Mordasini, C., van Boekel, R., Mollière, P., Henning, T., & Benneke, B. 2016, *ApJ*, 832, 41, doi: [10.3847/0004-637X/832/1/41](https://doi.org/10.3847/0004-637X/832/1/41)

- Morton, T. D., Bryson, S. T., Coughlin, J. L., et al. 2016, *ApJ*, 822, 86, doi: [10.3847/0004-637X/822/2/86](https://doi.org/10.3847/0004-637X/822/2/86)
- Moses, J. I., Madhusudhan, N., Visscher, C., & Freedman, R. S. 2013, *ApJ*, 763, 25, doi: [10.1088/0004-637X/763/1/25](https://doi.org/10.1088/0004-637X/763/1/25)
- Nielsen, E. L., De Rosa, R. J., Macintosh, B., et al. 2019, *AJ*, 158, 13, doi: [10.3847/1538-3881/ab16e9](https://doi.org/10.3847/1538-3881/ab16e9)
- Öberg, K. I., Murray-Clay, R., & Bergin, E. A. 2011, *ApJL*, 743, L16, doi: [10.1088/2041-8205/743/1/L16](https://doi.org/10.1088/2041-8205/743/1/L16)
- O'Donovan, F. T., Charbonneau, D., Bakos, G. Á., et al. 2007, *ApJL*, 663, L37, doi: [10.1086/519793](https://doi.org/10.1086/519793)
- Pál, A., Bakos, G. Á., Torres, G., et al. 2008, *ApJ*, 680, 1450, doi: [10.1086/588010](https://doi.org/10.1086/588010)
- Palma-Bifani, P., Chauvin, G., Bonnefoy, M., et al. 2022, arXiv e-prints, arXiv:2211.01474, <https://arxiv.org/abs/2211.01474>
- Pelletier, S., Benneke, B., Darveau-Bernier, A., et al. 2021, *AJ*, 162, 73, doi: [10.3847/1538-3881/ac0428](https://doi.org/10.3847/1538-3881/ac0428)
- Perryman, M. A. C., Lindegren, L., Kovalevsky, J., et al. 1997, *A&A*, 323, L49
- Petrus, S., Bonnefoy, M., Chauvin, G., et al. 2020, *A&A*, 633, A124, doi: [10.1051/0004-6361/201935732](https://doi.org/10.1051/0004-6361/201935732)
- . 2021, *A&A*, 648, A59, doi: [10.1051/0004-6361/202038914](https://doi.org/10.1051/0004-6361/202038914)
- Petrus, S., Chauvin, G., Bonnefoy, M., et al. 2023, *A&A*, 670, L9, doi: [10.1051/0004-6361/202244494](https://doi.org/10.1051/0004-6361/202244494)
- Pinhas, A., Madhusudhan, N., Gandhi, S., & MacDonald, R. 2019, *MNRAS*, 482, 1485, doi: [10.1093/mnras/sty2544](https://doi.org/10.1093/mnras/sty2544)
- Pont, F., Endl, M., Cochran, W. D., et al. 2010, *MNRAS*, 402, L1, doi: [10.1111/j.1745-3933.2009.00785.x](https://doi.org/10.1111/j.1745-3933.2009.00785.x)
- Rameau, J., Chauvin, G., Lagrange, A. M., et al. 2013, *A&A*, 553, A60, doi: [10.1051/0004-6361/201220984](https://doi.org/10.1051/0004-6361/201220984)
- Rasio, F. A., & Ford, E. B. 1996, *Science*, 274, 954, doi: [10.1126/science.274.5289.954](https://doi.org/10.1126/science.274.5289.954)
- Rickman, E. L., Matthews, E., Ceva, W., et al. 2022, *A&A*, 668, A140, doi: [10.1051/0004-6361/202244633](https://doi.org/10.1051/0004-6361/202244633)
- Rosenthal, L. J., Fulton, B. J., Hirsch, L. A., et al. 2021, *ApJS*, 255, 8, doi: [10.3847/1538-4365/abe23c](https://doi.org/10.3847/1538-4365/abe23c)
- Ruffio, J.-B., Macintosh, B., Konopacky, Q. M., et al. 2019, *AJ*, 158, 200, doi: [10.3847/1538-3881/ab4594](https://doi.org/10.3847/1538-3881/ab4594)
- Ruffio, J.-B., Konopacky, Q. M., Barman, T., et al. 2021, arXiv e-prints, arXiv:2109.07614, <https://arxiv.org/abs/2109.07614>
- Santos, N. C., Adibekyan, V., Figueira, P., et al. 2017, *A&A*, 603, A30, doi: [10.1051/0004-6361/201730761](https://doi.org/10.1051/0004-6361/201730761)
- Schlaufman, K. C. 2018, *ApJ*, 853, 37, doi: [10.3847/1538-4357/aa961c](https://doi.org/10.3847/1538-4357/aa961c)
- Sepulveda, A. G., & Bowler, B. P. 2022, *AJ*, 163, 52, doi: [10.3847/1538-3881/ac3bb5](https://doi.org/10.3847/1538-3881/ac3bb5)
- Sing, D. K., Fortney, J. J., Nikolov, N., et al. 2016, *Nature*, 529, 59, doi: [10.1038/nature16068](https://doi.org/10.1038/nature16068)
- Siverd, R. J., Beatty, T. G., Pepper, J., et al. 2012, *ApJ*, 761, 123, doi: [10.1088/0004-637X/761/2/123](https://doi.org/10.1088/0004-637X/761/2/123)
- Skemer, A. J., Hinz, P. M., Esposito, S., et al. 2012, *ApJ*, 753, 14, doi: [10.1088/0004-637X/753/1/14](https://doi.org/10.1088/0004-637X/753/1/14)
- Smalley, B., Anderson, D. R., Collier-Cameron, A., et al. 2012, *A&A*, 547, A61, doi: [10.1051/0004-6361/201219731](https://doi.org/10.1051/0004-6361/201219731)
- Stassun, K. G., Collins, K. A., & Gaudi, B. S. 2017, *AJ*, 153, 136, doi: [10.3847/1538-3881/aa5df3](https://doi.org/10.3847/1538-3881/aa5df3)
- Stassun, K. G., Oelkers, R. J., Paegert, M., et al. 2019, *AJ*, 158, 138, doi: [10.3847/1538-3881/ab3467](https://doi.org/10.3847/1538-3881/ab3467)
- Teske, J. K., Cunha, K., Schuler, S. C., Griffith, C. A., & Smith, V. V. 2013a, *ApJ*, 778, 132, doi: [10.1088/0004-637X/778/2/132](https://doi.org/10.1088/0004-637X/778/2/132)
- Teske, J. K., Schuler, S. C., Cunha, K., Smith, V. V., & Griffith, C. A. 2013b, *ApJL*, 768, L12, doi: [10.1088/2041-8205/768/1/L12](https://doi.org/10.1088/2041-8205/768/1/L12)
- Theissen, C. A., Konopacky, Q. M., Lu, J. R., et al. 2022, *ApJ*, 926, 141, doi: [10.3847/1538-4357/ac3252](https://doi.org/10.3847/1538-4357/ac3252)
- Thiabaud, A., Marboeuf, U., Alibert, Y., Leya, I., & Mezger, K. 2015, *A&A*, 574, A138, doi: [10.1051/0004-6361/201424868](https://doi.org/10.1051/0004-6361/201424868)
- Thorsbro, B., Ryde, N., Schultheis, M., et al. 2018, *ApJ*, 866, 52, doi: [10.3847/1538-4357/aadb97](https://doi.org/10.3847/1538-4357/aadb97)
- Toomre, A. 1964, *ApJ*, 139, 1217, doi: [10.1086/147861](https://doi.org/10.1086/147861)
- Tsiaras, A., Waldmann, I. P., Rocchetto, M., et al. 2016, *ApJ*, 832, 202, doi: [10.3847/0004-637X/832/2/202](https://doi.org/10.3847/0004-637X/832/2/202)
- Tsiaras, A., Waldmann, I. P., Zingales, T., et al. 2018, *AJ*, 155, 156, doi: [10.3847/1538-3881/aaaf75](https://doi.org/10.3847/1538-3881/aaaf75)
- van der Marel, N., Bosman, A. D., Krijt, S., Mulders, G. D., & Bergner, J. B. 2021, *A&A*, 653, L9, doi: [10.1051/0004-6361/202141786](https://doi.org/10.1051/0004-6361/202141786)
- Vigan, A., Fontanive, C., Meyer, M., et al. 2021, *A&A*, 651, A72, doi: [10.1051/0004-6361/202038107](https://doi.org/10.1051/0004-6361/202038107)
- Visscher, C., & Fegley, Bruce, J. 2005, *ApJ*, 623, 1221, doi: [10.1086/428493](https://doi.org/10.1086/428493)
- Wang, J., Wang, J. J., Ruffio, J.-B., et al. 2023, *AJ*, 165, 4, doi: [10.3847/1538-3881/ac9f19](https://doi.org/10.3847/1538-3881/ac9f19)
- Wang, Y.-H., Wang, S., Hinse, T. C., et al. 2019, *AJ*, 157, 82, doi: [10.3847/1538-3881/aaf6b6](https://doi.org/10.3847/1538-3881/aaf6b6)
- Weidenschilling, S. J., & Marzari, F. 1996, *Nature*, 384, 619, doi: [10.1038/384619a0](https://doi.org/10.1038/384619a0)
- West, R. G., Hellier, C., Almenara, J. M., et al. 2016, *A&A*, 585, A126, doi: [10.1051/0004-6361/201527276](https://doi.org/10.1051/0004-6361/201527276)
- Wilcomb, K. K., Konopacky, Q. M., Barman, T. S., et al. 2020, *AJ*, 160, 207, doi: [10.3847/1538-3881/abb9b1](https://doi.org/10.3847/1538-3881/abb9b1)
- Wilson, D. M., Gillon, M., Hellier, C., et al. 2008, *ApJL*, 675, L113, doi: [10.1086/586735](https://doi.org/10.1086/586735)

- Woitke, P., Helling, C., Hunter, G. H., et al. 2018, *A&A*, 614, A1, doi: [10.1051/0004-6361/201732193](https://doi.org/10.1051/0004-6361/201732193)
- Wong, M. H., Mahaffy, P. R., Atreya, S. K., Niemann, H. B., & Owen, T. C. 2004, *Icarus*, 171, 153, doi: [10.1016/j.icarus.2004.04.010](https://doi.org/10.1016/j.icarus.2004.04.010)
- Zhang, Y., Snellen, I. A. G., Bohn, A. J., et al. 2021, *Nature*, 595, 370, doi: [10.1038/s41586-021-03616-x](https://doi.org/10.1038/s41586-021-03616-x)
- Zhou, G., Huang, C. X., Bakos, G. Á., et al. 2019, *AJ*, 158, 141, doi: [10.3847/1538-3881/ab36b5](https://doi.org/10.3847/1538-3881/ab36b5)
- Zuckerman, B., Rhee, J. H., Song, I., & Bessell, M. S. 2011, *ApJ*, 732, 61, doi: [10.1088/0004-637X/732/2/61](https://doi.org/10.1088/0004-637X/732/2/61)
- Zurlo, A., Vigan, A., Galicher, R., et al. 2016, *A&A*, 587, A57, doi: [10.1051/0004-6361/201526835](https://doi.org/10.1051/0004-6361/201526835)
- Zurlo, A., Goździewski, K., Lazzoni, C., et al. 2022, *A&A*, 666, A133, doi: [10.1051/0004-6361/202243862](https://doi.org/10.1051/0004-6361/202243862)